



Article

Development of Novel Class of Phenylpyrazolo[3,4-*d*]pyrimidine-Based Analogs with Potent Anticancer Activity and Multitarget Enzyme Inhibition Supported by Docking Studies

Ahmed K. B. Aljohani ^{1,†}, Waheed Ali Zaki El Zaloo ^{2,†}, Mohamed Alswah ^{2,*}, Mohamed A. Seleem ², Mohamed M. Elsebaei ², Ashraf H. Bayoumi ², Ahmed M. El-Morsy ^{2,3}, Mohammed Almaghrabi ¹, Aeshah A. Awaji ⁴, Ali Hammad ², Marwa Alsulaimany ¹ and Hany E. A. Ahmed ^{2,*}

- ¹ Pharmacognosy and Pharmaceutical Chemistry Department, College of Pharmacy, Taibah University, Al-Madinah Al-Munawarah 41477, Saudi Arabia; akjohani@taibahu.edu.sa (A.K.B.A.); mhmaghrabi@taibahu.edu.sa (M.A.); msulaimany@taibahu.edu.sa (M.A.)
- ² Pharmaceutical Organic Chemistry Department, Faculty of Pharmacy, Al-Azhar University, Cairo 11884, Egypt; m.seleem@azhar.edu.eg (M.A.S.); m.elsebaei@azhar.edu.eg (M.M.E.); ashraf.bayoumi@azhar.edu.eg (A.H.B.); ahmedelmorsy232@yahoo.com (A.M.E.-M.); alihammad@azhar.edu.eg (A.H.)
- ³ Pharmaceutical Chemistry Department, College of Pharmacy, The Islamic University, Najaf 54001, Iraq
- ⁴ Department of Biology, Faculty of Science, University College of Taymaa, University of Tabuk, Tabuk 71491, Saudi Arabia; aawaji@ut.edu.sa
- * Correspondence: drmohammedalswah@azhar.edu.eg (M.A.); heahmad@azhar.edu.eg (H.E.A.A.)
- † They both made an equal contribution to the study and share the first authorship.



Citation: Aljohani, A.K.B.; El Zaloo, W.A.Z.; Alswah, M.; Seleem, M.A.; Elsebaei, M.M.; Bayoumi, A.H.; El-Morsy, A.M.; Almaghrabi, M.; Awaji, A.A.; Hammad, A.; et al. Development of Novel Class of Phenylpyrazolo[3,4-*d*]pyrimidine-Based Analogs with Potent Anticancer Activity and Multitarget Enzyme Inhibition Supported by Docking Studies. *Int. J. Mol. Sci.* **2023**, *24*, 15026. <https://doi.org/10.3390/ijms241915026>

Academic Editor: Guan-Jhong Huang

Received: 20 September 2023
Revised: 26 September 2023
Accepted: 27 September 2023
Published: 9 October 2023



Copyright: © 2023 by the authors. Licensee MDPI, Basel, Switzerland. This article is an open access article distributed under the terms and conditions of the Creative Commons Attribution (CC BY) license (<https://creativecommons.org/licenses/by/4.0/>).

Abstract: Phenylpyrazolo[3,4-*d*]pyrimidine is considered a milestone scaffold known to possess various biological activities such as antiparasitic, antifungal, antimicrobial, and antiproliferative activities. In addition, the urgent need for selective and potent novel anticancer agents represents a major route in the drug discovery process. Herein, new aryl analogs were synthesized and evaluated for their anticancer effects on a panel of cancer cell lines: MCF-7, HCT116, and HePG-2. Some of these compounds showed potent cytotoxicity, with variable degrees of potency and cell line selectivity in antiproliferative assays with low resistance. As the analogs carry the pyrazolopyrimidine scaffold, which looks structurally very similar to tyrosine and receptor kinase inhibitors, the potent compounds were evaluated for their inhibitory effects on three essential cancer targets: EGFR^{WT}, EGFR^{T790M}, VGFR2, and Top-II. The data obtained revealed that most of these compounds were potent, with variable degrees of target selectivity and dual EGFR/VGFR2 inhibitors at the IC₅₀ value range, i.e., 0.3–24 μM. Among these, compound **5i** was the most potent non-selective dual EGFR/VGFR2 inhibitor, with inhibitory concentrations of 0.3 and 7.60 μM, respectively. When **5i** was tested in an MCF-7 model, it effectively inhibited tumor growth, strongly induced cancer cell apoptosis, inhibited cell migration, and suppressed cell cycle progression leading to DNA fragmentation. Molecular docking studies were performed to explore the binding mode and mechanism of such compounds on protein targets and mapped with reference ligands. The results of our studies indicate that the newly discovered phenylpyrazolo[3,4-*d*]pyrimidine-based multitarget inhibitors have significant potential for anticancer treatment.

Keywords: phenylpyrazolo[3,4-*d*]pyrimidine; tyrosine kinase; cell cycle analysis; EGFR; VGFR; apoptosis; docking

1. Introduction

Cancer is a significant and prevalent health issue and is one of the leading causes of death globally [1,2]. This disease is characterized by sustained proliferative potential, growth signals,

and self-sufficiency, with apoptotic and antiproliferative cues resistance [3–5]. There have been advancements in diagnosing cancer early and the development of new treatments; however, there is still a lack of effective therapeutics for treating advanced cancers [6]. As conventional methods for treatment of cancer, radio and chemotherapy are no longer effective due to several side effects, including the unbiased destruction of body cells at comparable rates [7,8]. Thus, multiple attempts have been made to treat advanced cancer cases utilizing targeted therapies [9,10].

For targeted anticancer therapies, the pyrazolo[3,4-*d*]pyrimidine scaffold has gained great recognition due to its diverse and versatile pharmacological potential and structural similarity to ATP cofactor [11–13]. This similarity urges the utilization of pyrazolo[3,4-*d*]pyrimidine as a bioisosteric replacement of adenine (9H-purin-6-amine) as it would keep the fundamental interactions at the kinase domain [14,15]. The extensive role of kinases in many reported illnesses encourages extensive work to design and deliver potent analogs of pyrazolo[3,4-*d*]pyrimidine [14,16–18]. Several derivatives have shown a distinct growth-inhibitory activity via CDK1, CDK2, and 5-lipoxygenase enzymes' inhibition [19,20]. Interesting drugs that bear this scaffold are Dinaciclib, ibrutinib, and roscovitine, with potent CDK2 inhibition [14,16–18].

The advancement of targeted therapies that aim to hinder or obstruct crucial cellular pathways in tumor growth and metastasis has led to a greater understanding of the diversity within tumors and their ability to circumvent the blockade of signaling pathways. Consequently, certain tumors may inherently display resistance or develop resistance to therapies that target a particular pathway. To address this challenge, employing a comprehensive strategy that involves the concise inhibition of multiple signaling pathways may be fruitful. This strategy can help counteract tumor resistance by blocking potential alternative paths for tumor escape [5,21–27].

Vascular endothelial growth factor (VEGF) and the epidermal growth factor receptor (EGFR) are complementary pathways that play a fundamental role in tumor survival and diffusion [28–30]. The VEGF signaling pathway is upregulated by the expression of EGFR, which contributes to cancer resistance. VEGF and EGFR can exaggerate tumors through the exertion of both indirect and direct effects on tumor cells [28]. Targeting both pathways via mono- or multi-target therapeutics demonstrates a potential clinical benefit in many cancerous conditions. It is worth noting that therapeutics that impact VEGF-related pathways may contribute to the therapeutic targeting of the EGFR pathway [21,31–34]. Dual inhibitors of VEGF/EGFR could potentially improve antitumor efficacy and overcome resistance.

1*H*-Pyrazolo[3,4-*d*]pyrimidine scaffold has been reported to be an essential pharmacophore in many anticancer agents [16,35,36], including EGFR-TKIs. Herein, given examples include compounds 1–8 (Figure 1), which were tested as anticancer agents with a pyrimidine-based library of the anti-EGFR-TK mechanism and have been approved by the FDA; these include first-generation examples such as erlotinib 1 and gefitinib 2; second-generation examples such as afatinib 3 and canertinib 4; third-generation EGFR-TKIs such as rociletinib 5, and avitinib 6; and clinical-phase compounds such as sapitinib 7 and dacomitinib 8.

The promising biological effects of 1*H*-pyrazolo[3,4-*d*]pyrimidine, in which the core scaffold was decorated with a pendant *N*-linker bonded to the aryl moiety at the 4 position, are able to consistently conserve activity against targets.

Other complexed examples of pyrazolo[3,4-*d*]pyrimidine-based EGFR-TK inhibitors (9–13) were discovered, with different potency profiles based on the ATP pharmacophore model. These compounds showed very interesting anticancer activity against specific cancer cell lines [37–40] (Figure 2).

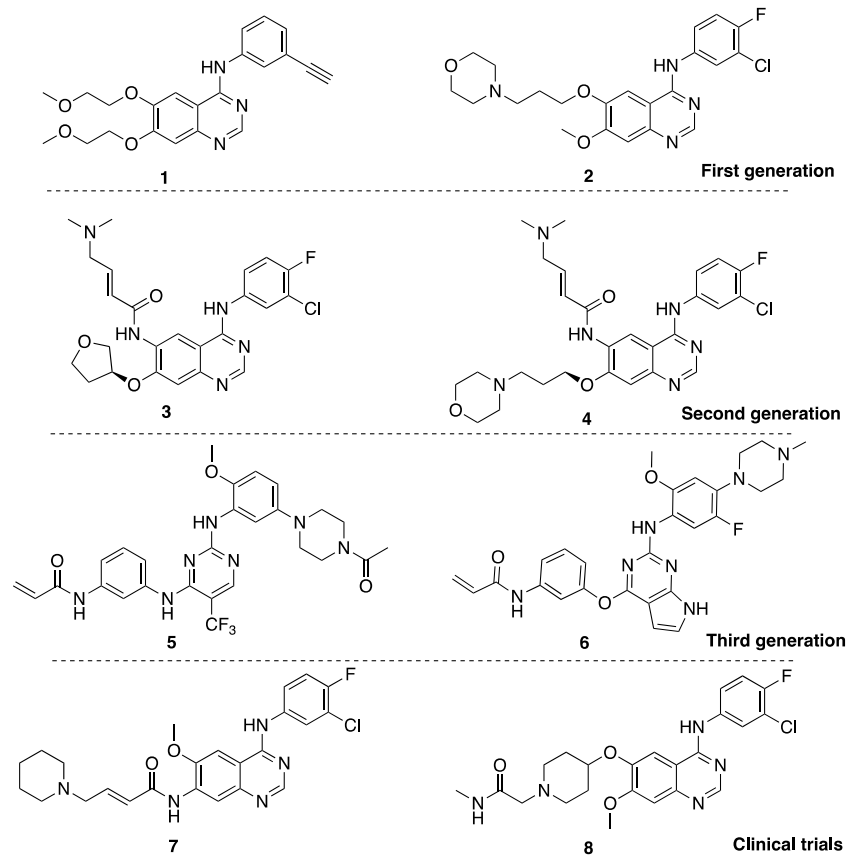


Figure 1. Examples of different generations of EGFR-TK inhibitors.

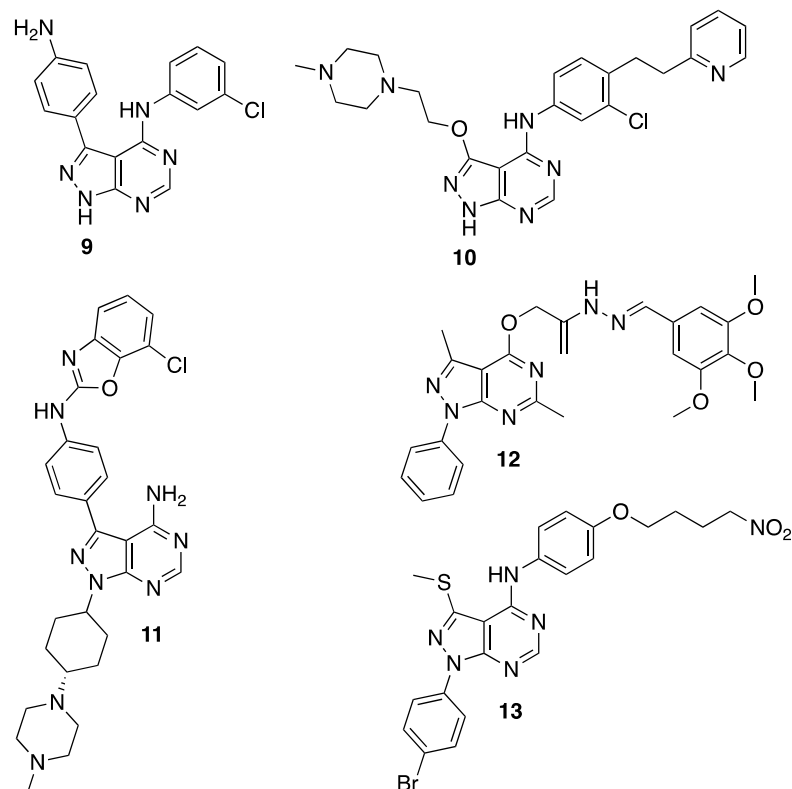


Figure 2. Examples of pyrazolo[3,4-d]pyrimidine-based EGFR-TK inhibitors.

2. Results and Discussion

2.1. Structure-Based Scaffold and Compound Design

Reports revealed that EGFR-TK is a polypeptide chain and that the ATP-binding groove of EGFR-TK is a 1186-amino-acids polypeptide chain. The ATP-binding region is composed of three areas: extracellular, intracellular, and hydrophobic regions (Figure 3a) [41,42]. SAR analysis of EGFR-TKIs revealed that they have four common pharmacophoric features. First, the core structure consists of a flat nitrogenous heterocycle. This ring occupies the adenine binding pocket and forms hydrogen bonding with Met793, Thr790, and Thr854. The next feature is represented by a terminal hydrophobic head (a plain or substituted phenyl group) that interacts with hydrophobic region I. Most of the reported inhibitors also bear a middle secondary amine group, occupying the linker region between the adenine binding region and the hydrophobic region. The final feature, represented by a hydrophobic tail, connects to the flat hetero aromatic ring system which occupies hydrophobic region II.

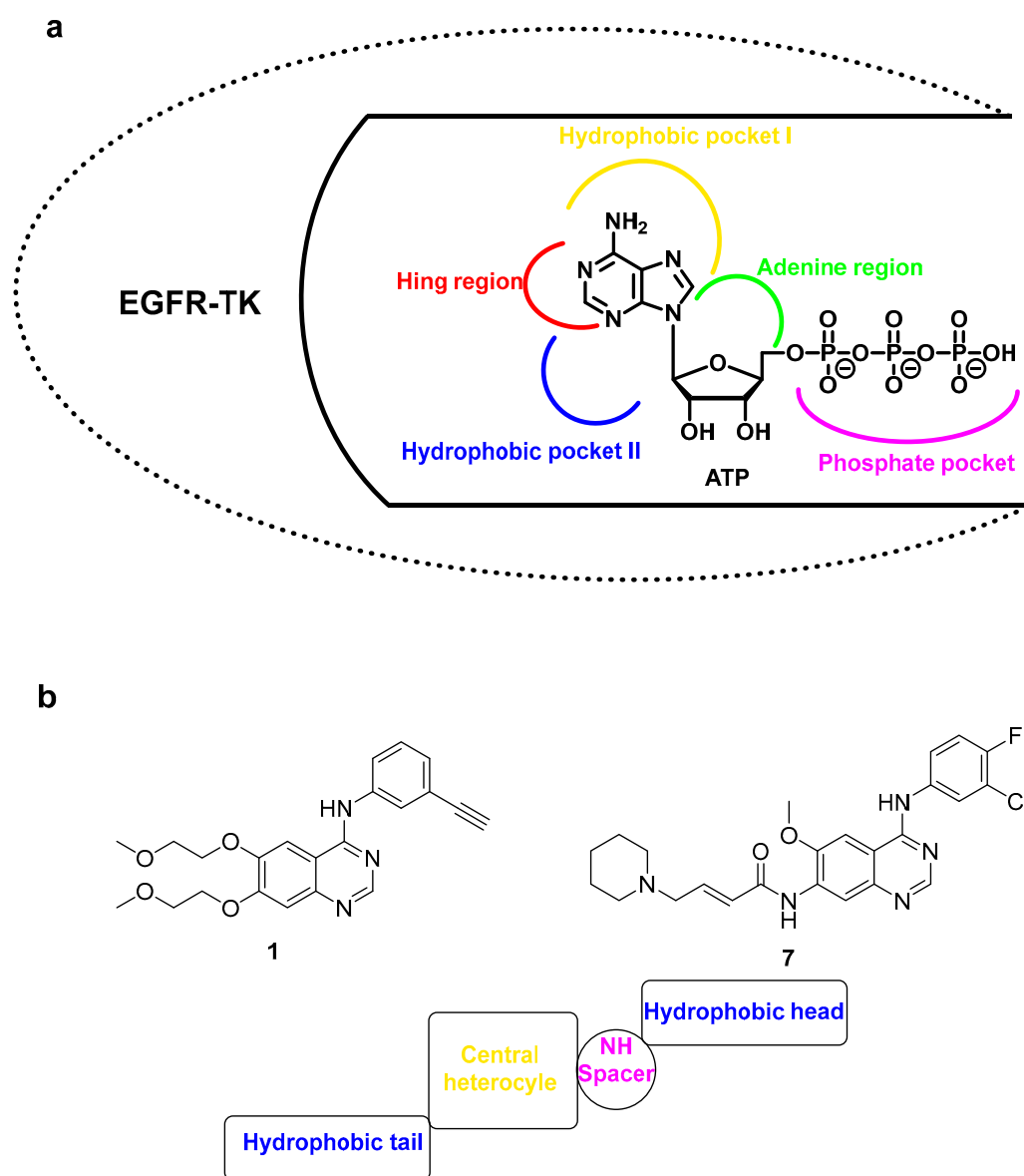


Figure 3. Work design. (a) Structure of ATP binding pocket, (b) Mapping of reference EGFR-TK inhibitors to pharmacophore points.

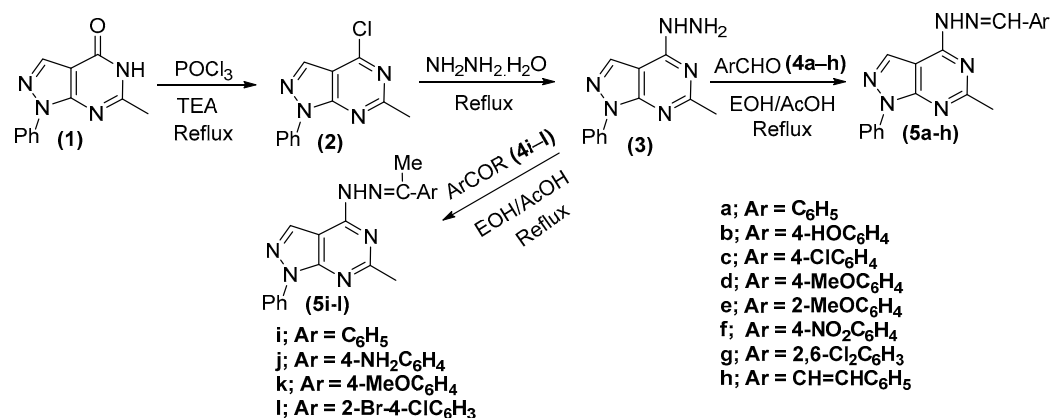
Based on the previous findings, we aimed to synthesize new 1*H*-pyrazolo[3,4-*d*]pyrimidine derivatives with potential anticancer activity. The target of this work was the synthesis of

new derivatives carrying the same essential pharmacophoric features of the reported EGFR-TKIs as compound **1** and compound **7** (Figure 3b). We used a bioisosteric replacement strategy to fill up the binding pocket in EGFR-TKIs at four different positions (Figure 3b). In the first position, we used 1*H*-pyrazolo[3,4-*d*]pyrimidine as a flat heterocyclic system as a bioisostere of the quinazoline core on compounds **1** and **7**. The suggested 1*H*-pyrazolo[3,4-*d*]pyrimidine core can fill the bulky space of the adenine-binding region (Figure 3a) [43,44]. The nitrogen atoms at the core would engage several hydrogen bonds, which would be translated into excellent EGFR-TK potency [44,45].

The second position and third regions consisted of two terminal hydrophobic regions represented by phenyl group position 1 and alkyl or aryl side chains connected to a nitrogenous spacer. The last part was the nitrogenous linker (spacer) region with various lengths and heteroatom contents (amine, hydrazide, or thiosemicarbazide). The suggested modifications we envisioned led to study the SAR of this scaffold as an anticancer agent through the inhibition of EGFR-TK.

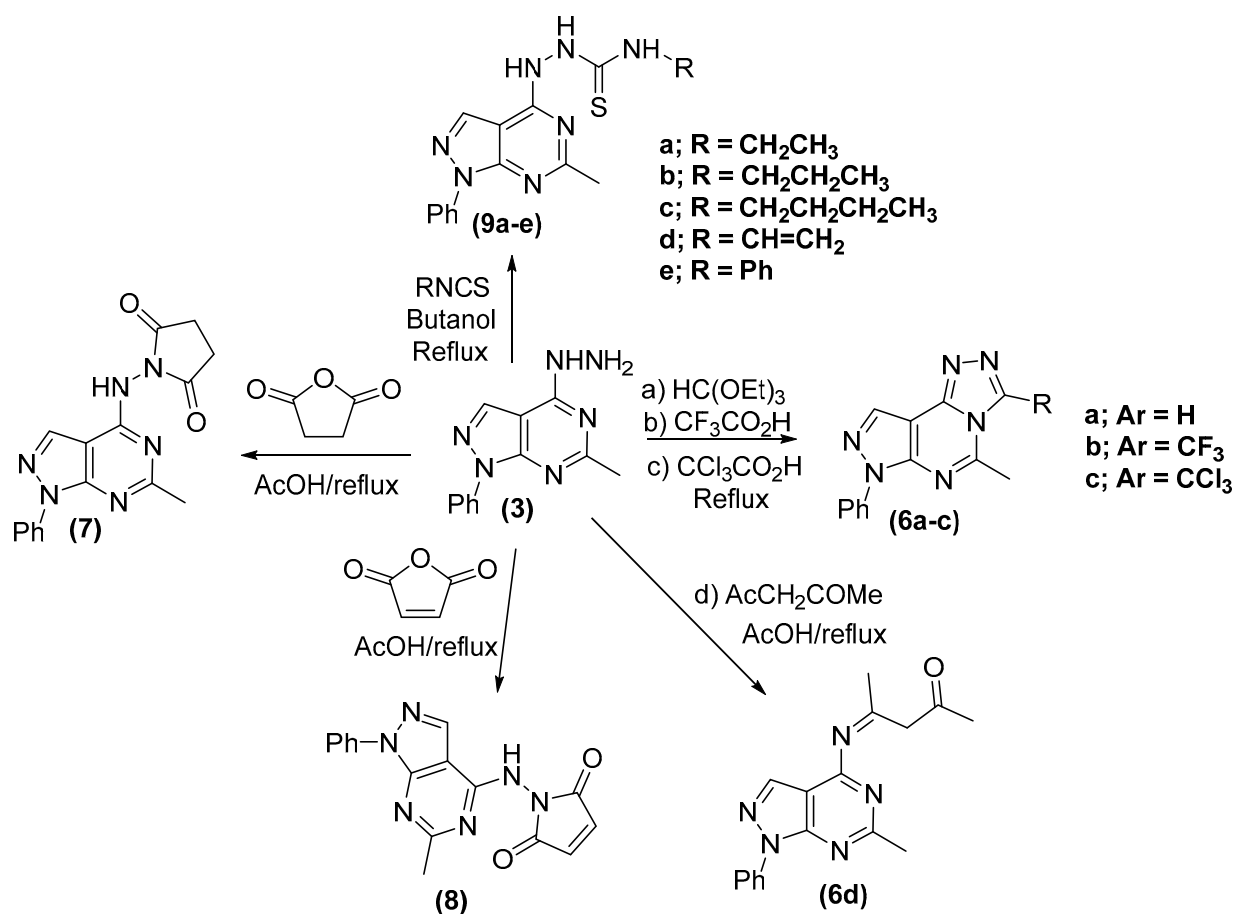
2.2. Chemistry

The route adopted for the synthesis of compounds **5a–l** and **6–9** is depicted in Schemes 1 and 2. Synthesis was initiated via chlorination of 6-methyl-1-phenyl-1,5-dihydro-4*H*-pyrazolo[3,4-*d*]pyrimidin-4-one (**1**) using phosphorous oxy-chloride in the presence of trimethylamine (TMA) to give the chlorinated derivative, 4-chloro-6-methyl-1-phenyl-1*H*-pyrazolo[3,4-*d*]pyrimidine (**2**). Hydrazinolysis of the 4-chloro derivative (**2**) under reflux gave the hydrazide derivative, 4-hydrazinyl-6-methyl-1-phenyl-1*H*-pyrazolo[3,4-*d*]pyrimidine (**3**). Condensation of compound **3** with appropriate aromatic aldehydes (**4a–h**) or acetophenones (**4i–l**) in ethanol and glacial acetic acid (as a catalyst) afforded the open chain Schiff base products, 4-(2-arylidenehydrazinyl)-6-methyl-1-phenyl-1*H*-pyrazolo[3,4-*d*]pyrimidine (**5a–l**).



Scheme 1. Synthetic protocol of 4-(2-arylidenehydrazinyl)-6-methyl-1-phenyl-1*H*-pyrazolo[3,4-*d*]pyrimidine (**5a–l**).

Next, we used 4-hydrazinyl-6-methyl-1-phenyl-1*H*-pyrazolo[3,4-*d*]pyrimidine (**3**) as a versatile intermediate to synthesize a variety of pyrazolo-triazolopyrimidine derivatives. Thus, refluxing of **3** with triethyl orthoformate, trifluoroacetic acid, and trichloroacetic acid, respectively, gave the following tricycle compounds; 5-methyl-7-phenyl-7*H*-pyrazolo[4,3-*e*][1,2,4]triazolo[4,3-*c*]pyrimidine (**6a**), 3-trifluoromethyl (**6b**) and 3-trichloromethyl (**6c**) derivatives, respectively, were formed. While condensation of **3** with acetyl acetone afforded the open-chain Schiff base product, 4-((6-Methyl-1-phenyl-1*H*-pyrazolo[3,4-*d*]pyrimidin-4-yl)imino)pentan-2-one (**6d**). Reaction of **3** with dihydrofuran-2,5-dione, furan-2,5-dione, and indoline-2,3-dione, respectively, afforded 1-((6-methyl-1-phenyl-1*H*-pyrazolo[3,4-*d*]pyrimidin-4-yl)amino)pyrrolidine-2,5-dione (**7**), 1-((6-methyl-1-phenyl-1*H*-pyrazolo[3,4-*d*]pyrimidin-4-yl)amino)-1*H*-pyrrole-2,5-dione (**8**), and 3-(2-(6-methyl-1-phenyl-1*H*-pyrazolo[3,4-*d*]pyrimidin-4-yl)hydrazono)indolin-2-one (**9**), respectively, as shown in the Scheme 2.



Scheme 2. Synthetic protocol of pyrazolopyrimidine derivatives (6–9).

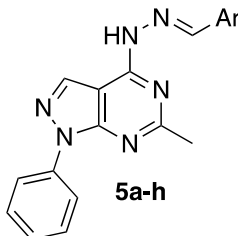
Finally, interaction of the hydrazinyl derivative (3) with several isothiocyanates, namely, ethyl isothiocyanate, propyl isothiocyanate, butyl isocyanate, vinyl isothiocyanate, and phenyl isothiocyanate, in butanol (20 mL) under reflux afforded the *N*-alkyl/aryl-2-(6-methyl-1-phenyl-1*H*-pyrazolo[3,4-*d*]pyrimidin-4-yl)hydrazinecarbothioamides (9a–e), respectively, as shown in the Scheme 2.

2.3. Anticancer Assay

The antiproliferative activity of the synthesized library was examined against three human cancer cell lines; breast (MCF-7), colon (HCT-116), and liver (HepG₂) utilizing an MTT assay with the human diploid fibroblasts (WI-38) normal cell line as a comparison [46–48]. The data are summarized in Table 1. According to our design, the tested compounds are classified into four categories based on the length and the chemotype of the spacer (Figure 3). In the first category, we used monosubstituted hydrazone linker. Among the tested derivatives in this category, compound 5b with *p*-hydroxyphenyl showed the most promising activity against the three cell lines when compared with the reference drug. Additionally, the *O*-methylated congeners, compounds 5d and e, maintained promising activity against HCT-116 cells with IC₅₀ 9.87 and 8.15 μM, respectively. The second category is represented by monosubstituted hydrazone linker. In this category, compound 5a, carrying the unsubstituted phenyl group, demonstrated noticeable activities against the three cell lines.

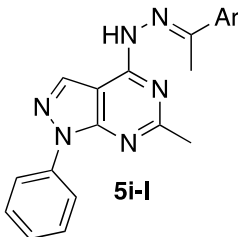
Table 1. Results of in vitro anticancer activity of the newly synthesized pyrazolopyrimidine compounds, IC₅₀ (μM).

| Compounds | Ar | HePG-2 | MCF-7 | HCT-116 | WI-38 |
|-----------|----|------------|------------|------------|--------------|
| DOX | | 4.50 ± 0.2 | 4.17 ± 0.2 | 5.23 ± 0.3 | 10.63 ± 0.47 |



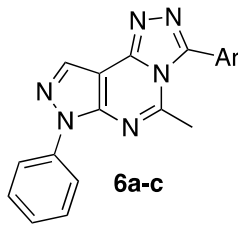
5a-h

| | | | | | |
|-----------|--|-------------|-------------|-------------|----------|
| 5a | C ₆ H ₅ | 15.10 ± 1.2 | 21.13 ± 1.5 | 11.69 ± 0.9 | |
| 5b | 4-OH-C ₆ H ₅ | 9.12 ± 0.7 | 10.48 ± 0.7 | 5.65 ± 0.3 | 35 ± 0.3 |
| 5c | 4-Cl-C ₆ H ₅ | 83.71 ± 4.4 | 66.61 ± 3.8 | 39.54 ± 2.6 | - |
| 5g | 2,6-Cl-C ₆ H ₅ | >100 | >100 | >100 | - |
| 5d | 4-OMe-C ₆ H ₅ | 18.34 ± 1.5 | 19.36 ± 1.3 | 9.87 ± 0.7 | - |
| 5e | 2-OMe-C ₆ H ₅ | 13.79 ± 1.0 | 16.07 ± 1.1 | 8.15 ± 0.5 | - |
| 5f | 4-NO ₂ -C ₆ H ₅ | >100 | >100 | 89.68 ± 4.8 | - |
| 5h | 4-CH=CH-C ₆ H ₅ | >100 | >100 | 76.84 ± 4.1 | - |



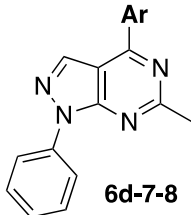
5i-l

| | | | | | |
|-----------|--|-------------|-------------|-------------|------|
| 5i | C ₆ H ₅ | 6.38 ± 0.1 | 3.81 ± 0.3 | 4.38 ± 0.2 | >100 |
| 5j | 4-NH ₂ -C ₆ H ₅ | 44.31 ± 2.9 | 36.04 ± 2.4 | 21.50 ± 1.5 | - |
| 5k | 4-OMe-C ₆ H ₅ | 91.63 ± 5.1 | 88.29 ± 4.7 | 78.05 ± 4.2 | - |
| 5l | 2-Br-4-Cl-C ₆ H ₅ | 17.08 ± 1.3 | 29.15 ± 1.8 | 14.59 ± 1.1 | - |



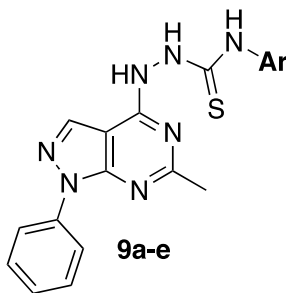
6a-c

| | | | | | |
|-----------|------------------|-------------|-------------|-------------|---|
| 6a | H | 37.50 ± 2.7 | 49.65 ± 3.1 | 34.60 ± 2.2 | - |
| 6b | CF ₃ | 25.16 ± 2.0 | 39.10 ± 2.5 | 26.06 ± 1.8 | - |
| 6c | CCl ₃ | 56.18 ± 3.5 | 54.19 ± 3.4 | 37.18 ± 2.4 | - |



6d-7-8

Table 1. Cont.

| Compounds | Ar | HePG-2 | MCF-7 | HCT-116 | WI-38 |
|---|---|-------------|-------------|-------------|-----------|
| 6d |  | 89.22 ± 4.7 | 84.58 ± 4.6 | 93.43 ± 5.2 | - |
| 7 |  | 87.21 ± 4.5 | 81.02 ± 4.6 | 73.50 ± 3.8 | - |
| 8 |  | 78.53 ± 4.3 | 79.46 ± 4.4 | 66.30 ± 3.5 | - |
|  9a-e | | | | | |
| 9a | -CH ₂ CH ₃ | 5.97 ± 0.3 | 7.61 ± 0.4 | 2.96 ± 0.1 | - |
| 9b | -CH ₂ CH ₂ CH ₃ | 23.88 ± 1.8 | 34.18 ± 2.0 | 17.59 ± 1.3 | - |
| 9c | - | 20.34 ± 1.6 | 31.42 ± 1.9 | 16.62 ± 1.2 | - |
| 9d | =CH ₂ | 32.61 ± 2.4 | 35.19 ± 2.2 | 19.72 ± 1.4 | - |
| 9e | Phenyl | 7.80 ± 0.4 | 8.99 ± 0.5 | 6.87 ± 0.5 | 66 ± 0.23 |

Possessing various chemical characteristics on scaffold dramatically ameliorated cytotoxic activity. In the third category, we tethered the linker to the pyrimidine ring to provide the triazolo[4,3-*c*]pyrimidine core. Using this strategy, we aimed to reduce rotation at this part to reduce the entropic penalty of the binding of the compound to EGFR-TK. The three derivatives showed moderate cytotoxic activities. Next, we used four heterocyclic substitutions to build the fourth category of our compounds (**6d–7**). None of these molecules exhibited any meaningful activity against the three cell lines. In the last category, we used a thiosemicarbazide linker connected to various aliphatic and aromatic side chains (**9a–e**) with prominent activity for analogs **9a** and **9e**. Collectively, this series displayed the best activity against the three tested cell lines in comparison with the other categories (Table 1). In addition, compound **9a**, with ethyl side chain, overrides the activity of Doxorubicin against the HCT-116 cell line. In addition, normotoxicity was assessed for the most active analogs—**5b**, **5i**, and **9e**—on the WI38 cell line, and they exhibited a very low effect, with IC₅₀ greater than 35 μM, which indicated a good safety profile.

Next, we investigated the cytotoxic activity of selected derivatives against the same cell lines using the extended treatment strategy. Using this strategy, we aimed to examine the resistance ability of the tested cell lines to our compounds after incubation for a long time. We realized that in comparison with doxorubicin, some tested compounds exhibited a time-dependent cytotoxic activity; for example, compound **5i**. On the other hand, we noted a transient partial loss of cytotoxic activity 48 h post-treatment, followed by improved activity in the last time point. Table 2 and Figure 4 summarize the relative cytotoxic activity of the selected derivatives.

Table 2. In vitro cytotoxic activity of selected compounds 48 and 72 h post-incubation.

| Cell Line | Time | 5b | 5i | 9e | Dox |
|-----------|------|-------------|------------|------------|------------|
| HePG-2 | 24 h | 9.12 ± 0.7 | 6.38 ± 0.1 | 7.80 ± 0.4 | 4.50 ± 0.2 |
| | 48 h | 7.60 ± 0.7 | 3.34 ± 0.2 | 8.28 ± 0.8 | 3.24 ± 0.2 |
| | 72 h | 5.16 ± 0.4 | 2.42 ± 0.2 | 5.93 ± 0.5 | 1.07 ± 0.1 |
| MCF-7 | 24 h | 10.48 ± 0.7 | 3.81 ± 0.3 | 8.99 ± 0.5 | 4.17 ± 0.2 |
| | 48 h | 9.82 ± 0.9 | 3.34 ± 0.2 | 8.16 ± 0.8 | 2.82 ± 0.1 |
| | 72 h | 5.16 ± 0.4 | 1.24 ± 0.3 | 7.45 ± 0.7 | 0.69 ± 0.1 |
| HCT116 | 24 h | 5.65 ± 0.3 | 4.38 ± 0.2 | 6.87 ± 0.5 | 5.23 ± 0.3 |
| | 48 h | 9.82 ± 0.9 | 4.01 ± 0.3 | 6.77 ± 0.4 | 4.07 ± 0.3 |
| | 72 h | 4.09 ± 0.3 | 2.76 ± 0.3 | 5.55 ± 0.4 | 2.79 ± 0.2 |

Data are presented as average IC₅₀ ± SD (μM) values for at least three experiments.

2.4. In Vitro Cancer Related Targets Inhibition Analysis

Multi-targeting is a useful anticancer strategy with superior therapeutic attributes. A variety of tumors, such as aggressive breast cancers, offer the overexpression of different cellular enzyme targets which are responsible for large tumor size, poor differentiation, and poor clinical outcomes [49–52]. Triazole hybrids were discovered to be multi-target EGFR^{WT}-, EGFR^{T790M}-, VEGFR-2-, and Topo II based-inhibitors, and they were evaluated for anticancer activity [53,54]. Moreover, examples of Pyrazolo[3,4-*d*]pyrimidine-based multitarget anticancer inhibitors were reported [55]. As seen in the data for the cytotoxicity of the newly synthesized analogs, only active candidate compounds **5b**, **5i**, and **9e** were tested against a panel of cancer-related targets, namely, EGFR, VEGFR-2, and Topo-II, compared to reference drugs. The results are summarized in (Table 3). We found that compound **5b** strongly and selectively inhibited EGFR activity in the lower range, with 20-fold target selectivity indices over VGFR-2 and 108-fold over Topo-II. Moreover, compound **5i** showed low selective and potent inhibition of EGFR^{WT} and EGFR^{T790M} over VGFR-2 and Topo-II, with 20/66 selectivity indices. Compound **9e** was moderately active against VGFR-2 and Topo-II targets, with selectivity indices of 21/31 over EGFR^{WT}. Overall, the scaffold pyrazolo[3,4-*d*]pyrimidine analogs showed different degrees of multitarget potent inhibitory activity, which might contribute to the discovery of anticancer agents.

Table 3. In vitro EGFR-2-, VEGFR-2-, and Topo-II-inhibitory effects of new candidate compounds **5b**, **5i**, and **9e** compared to reference drugs.

| Compound | IC ₅₀ (μM) | | | |
|------------------|-----------------------|-----------------------|---------------|--------------|
| | EGFR ^{WT} | EGFR ^{T790M} | VGFR2 | Topo-II |
| 5b | 0.78 ± 0.02 | 1.93 ± 0.08 | 15.7 ± 0.32 | 108.3 ± 2.20 |
| 5i | 0.37 ± 0.18 | 0.56 ± 0.04 | 7.60 ± 0.15 | 24.7 ± 0.51 |
| 9e | 0.77 ± 0.018 | - | 16.24 ± 0.36 | 24.6 ± 0.54 |
| Etoposide | - | - | - | 33.6 ± 1.16 |
| Sorafenib | - | - | 0.073 ± 0.002 | - |
| Erlotinib | 0.13 ± 0.003 | 0.035 ± 0.001 | - | - |

Data are presented as average IC₅₀ ± SD (μM) values for at least three experiments. (-) not tested.

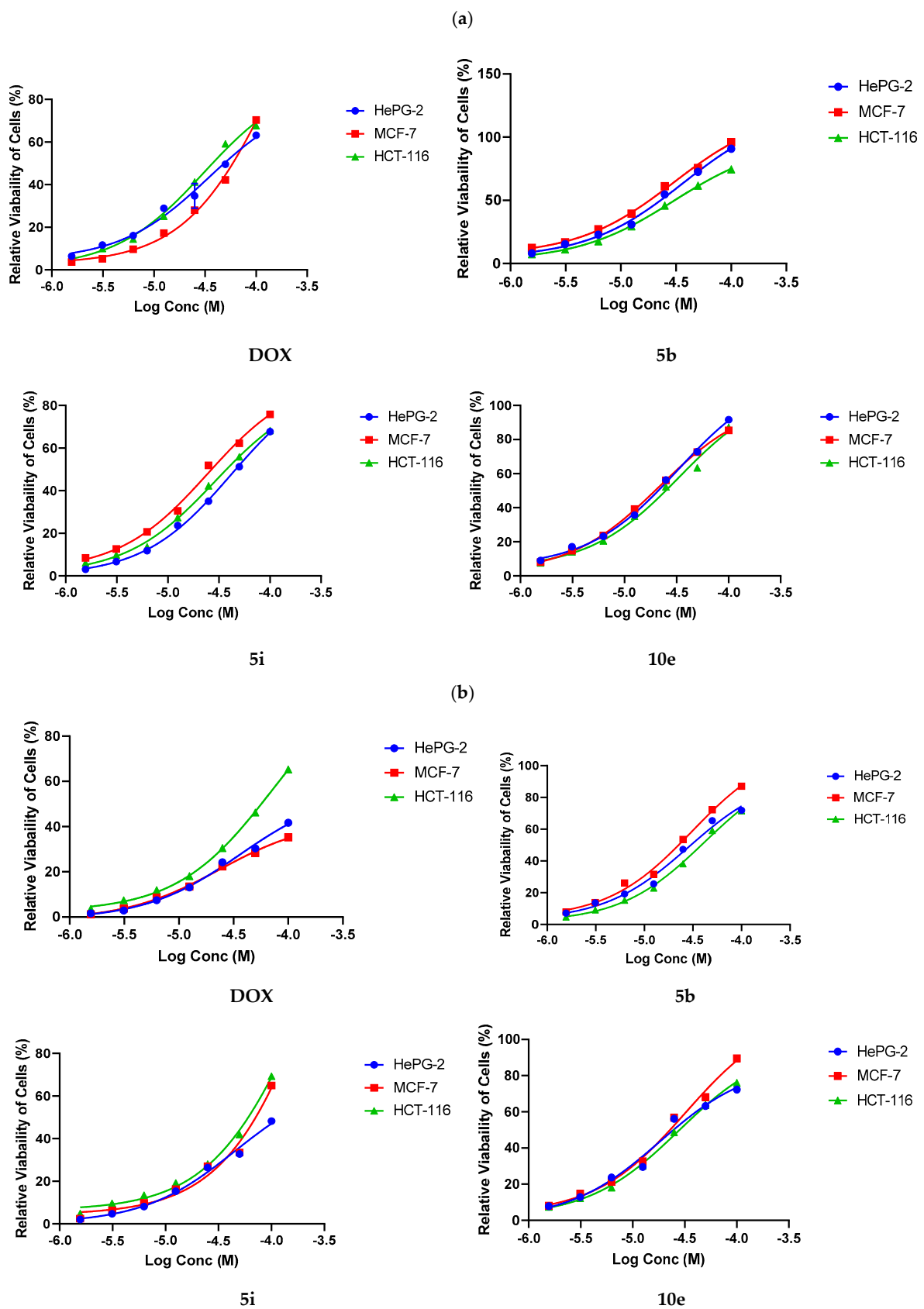


Figure 4. Cont.

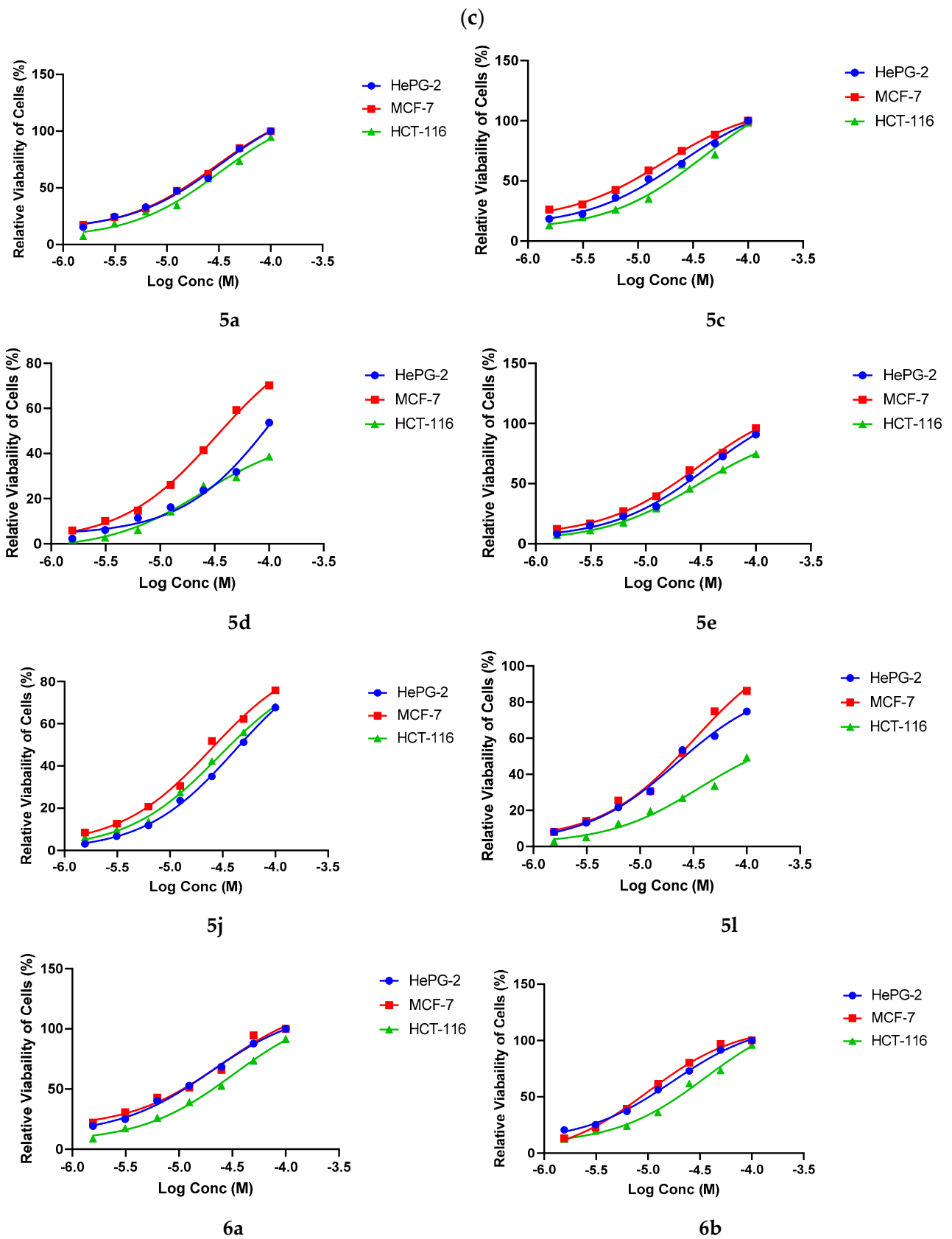


Figure 4. Cont.

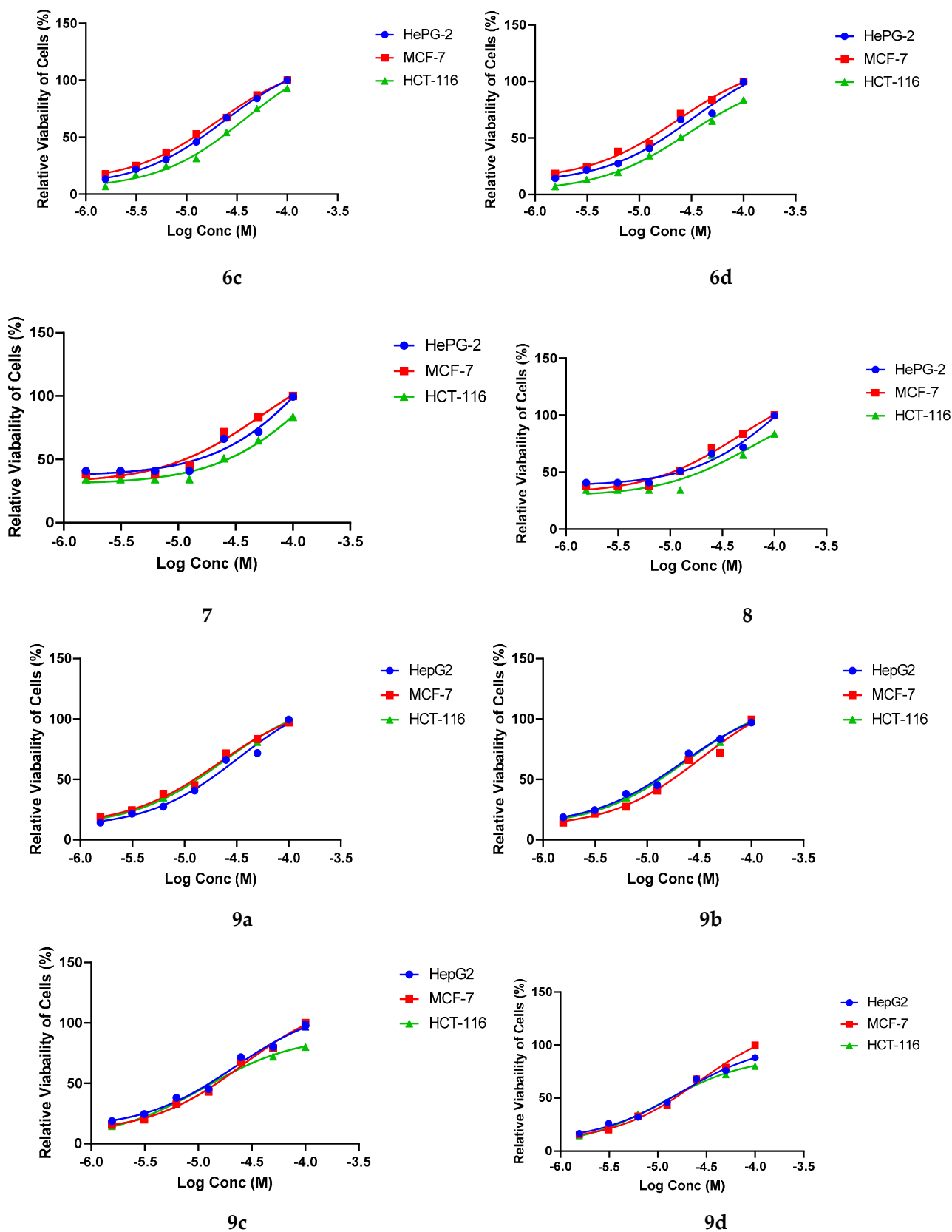


Figure 4. Relative cytotoxic activity of the selected molecules upon incubation with the selected cell lines for 48 h (a), 72 h (b), and 24 h (c).

2.5. Cell Cycle Analysis

Based on its antiproliferative activity, compound **5i** was designated for further studies to explore its effect on the induction of apoptosis in the A549 cell line [56]. We used this assay to elucidate the relationship between the proliferation inhibition and the cell cycle arrest, as well as to determine the biological phase in which the molecule interferes with cell growth. The cells were treated with 1 μ M of **5i**, and we used DMSO as a negative control. As presented in Figure 5, the data showed obvious interference with the native cell cycle distribution. Exposure of MCF-7 cells to our compound caused a decrease in the proportion of cells in the G₀/G₁ phase (from 57.39% to 49.63% when compared with the control). Moreover, it showed a slight increase in cell percentage in the S phase (from 33.97% to 43.12%), accompanied by a slight increase in the percentage of cells at the G₂/M phase of the cell cycle (from 8.64% in the control to 7.25%) and a significant increase in the pre-G₁ phase of the cell cycle (from 1.79% in the control to 36.06%). Collectively, these results indicated that compound **5i** can lead to apoptosis through arresting the G₁/S phase of cell cycle.

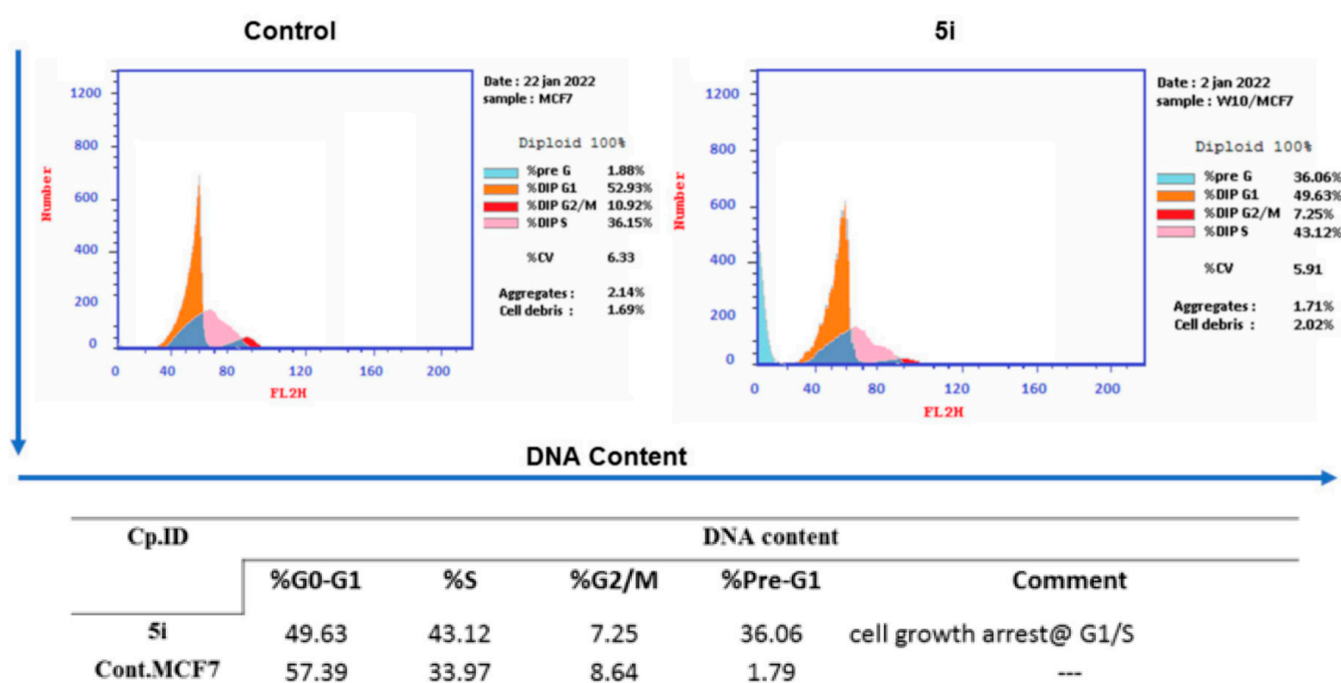


Figure 5. Dot plot of Annexin V/PI double staining of MCF-7 control and treatment with analogue **5i**. Statistical analysis of the apoptosis percentage of MCF-7 cells after incubation with compounds **5i** in conc. (3.81 μ M) for 24 h. The data are reported as the mean \pm SD of three independent experiments in triplicate.

2.6. Annexin V-FITC Apoptosis Assay

We used annexin V-binding studies via flow cytometer to confirm the apoptosis induction by our compound. The apoptotic nature of **5i** against MCF-7 cells was tested via flow cytometry detection after double-staining with Annexin V-FITC and propidium iodide (PI) [57]. The results demonstrated that the treatment of A549 cells with our compound for 48 h increased the early apoptosis ratio (lower right quadrant of the cytogram) from 0.44% to 12.62% and increased the late apoptosis ratio (higher right quadrant of the cytogram) from 0.17% to 19.11%, indicating that **5i** can induce MCF-7 cells apoptosis. In addition, treatment of MCF-7 cells with our compound for 24 h resulted in 36.06% of apoptotic cells (early + late) versus 1.79% of apoptotic cells in the untreated control (Figure 6). These results demonstrated that **5i** might inhibit cell growth through cell apoptosis induction.

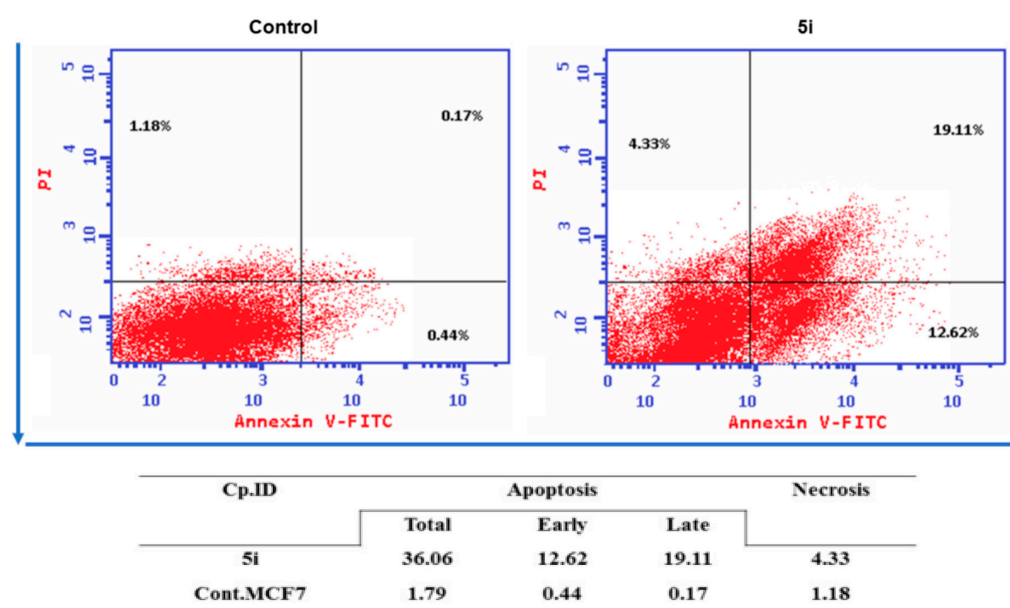


Figure 6. DNA content distribution histograms of control and treated cells. Statistical analysis of cell cycle phases percentage of MCF-7 cells after incubation with compound **5i** (3.81 μ M) for 24 h. The data are reported as the mean \pm SD of three independent experiments in triplicate.

2.7. EGFR/VEGFR2 Target Docking Simulations

The integration of experimental and computational methods is an attractive strategy by which to design and optimize successful drug candidates [32,34,51,52]. Based on the biological activity of **5i**, we carried out molecular docking studies as a crucial step to understand the mode of interaction of our selected molecule. First, a docking study was performed against EGFR (PDB ID: 1M17) (Figure 7a). Our compound was compared with erlotinib (compound **1**, Figure 1), the known EGFR inhibitor. Previous studies [34,58] have indicated that erlotinib causes EGFR inhibition by binding to the site occupied by ATP during phosphotransfer. The N¹ of the quinazoline accepts the hydrogen bond from the Met769 amide nitrogen. It has been reported that 1-diphenyl-4,5-dihydro-1H-pyrazolo[3,4-d]pyrimidin-6-amine scaffold has successfully tolerated the EGFR pocket [59]. Our data indicated that compound **5i** conserved the same interaction with Met769 as the reference molecule. The N¹ of the pyrazole ring formed a hydrogen bond with Met 769, with a distance of 0.8 Å. Furthermore, the pyrazolo[3,4-d]pyrimidine moiety was incorporated into pi–pi interaction with Gly772 and Cys773, respectively. The peripheral phenyl group of **5i** was buried inside hydrophobic region I. Additionally, a computational docking study was performed against VEGFR-2 (PDB ID: 3EWH) in comparison with a pyridyl-pyrimidine benzimidazole inhibitor (Figure 7b). The binding pattern of our molecule includes the pi–pi interaction of the core phenyl group with Leu1035 and the pyrimidine moiety with Lys868. Moreover, the hydrazide linker showed hydrogen bonding with Glu885, with a distance of 2.86 Å. This interaction imitates the same binding of the reference molecule with Glu885. A comparison of our molecule with both reference molecules through 2D molecular alignment revealed that **5i** occupies the same space in both receptors. In addition, a mapping experiment on an active **5i** analog referencing selective EGFR and VEGFR-2 compounds led to the discovery of conserved molecular motifs that contributed strongly to the binding mechanism and hence to biological activity (Figure 8).

2.8. Prediction of Drug-Likeness and ADME Properties

We used the OSIRIS Property Explorer to predict any potential side effects of our molecules, such as mutagenic, tumorigenic, irritant, and reproductive effects. Moreover, we tested a group of drug-relevant properties, including cLogP, LogS (solubility), MW, drug-likeness, and overall drug-score. The in silico physicochemical and toxicological analyses

were carried out with the OSIRIS Property Explorer program with respect to the two potent active analogs, **5b** and **5i**, compared to the two reported anticancer drugs. Properties with a high risk of undesirable effects, such as mutagenicity, tumorigenicity, irritant effects, and effects on reproductive physiology, as well as drug-relevant properties, including cLogP, LogS (solubility), MW, drug-likeness, and overall drug-score, are scored and color-coded, as shown in Table 4. The data of toxicity risks (shown in colors as red (high risk) and green (zero risk)) indicate a behavior consistent with the compound. Interestingly, the potential drug-likeness values of compounds **5i** and **5b** (4.26 and 3.97) were significantly higher than the two reference drugs, which showed negative values of -4.2 and -6.73 . However, the in silico prediction of the OSIRIS Property Explorer showed that the introduction of 4-OH on the aryl ring can retain the lack of tumorigenic and mutagenic toxicity risk and enhance the druggability of compound **5i** compared to the low-active one. In addition, we can see that both **5i** and **5b** compounds present a very excellent safety profile against all side effects. Generally, the drug-score values of compounds **5b** and **5i** (0.66 and 0.58) were better than those of sorafenib and erlotinib (0.20 and 0.38). It was noted via %ABS that analog **5i** was 85% better than the others. The reasons for this good analysis are the absence of reactive functional groups within the chemical structure, the chemical stability, and the simplicity in the formula.

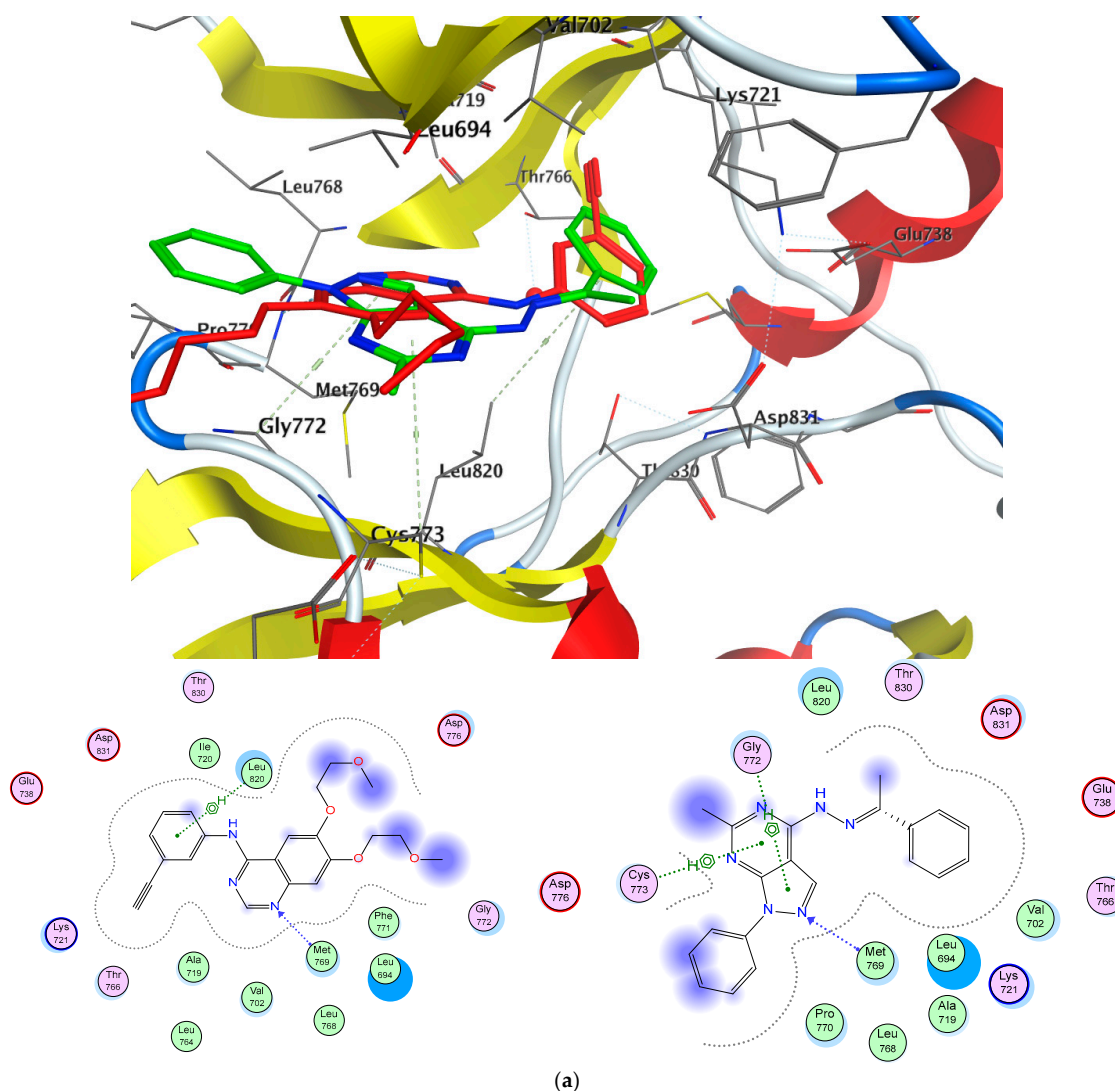


Figure 7. Cont.

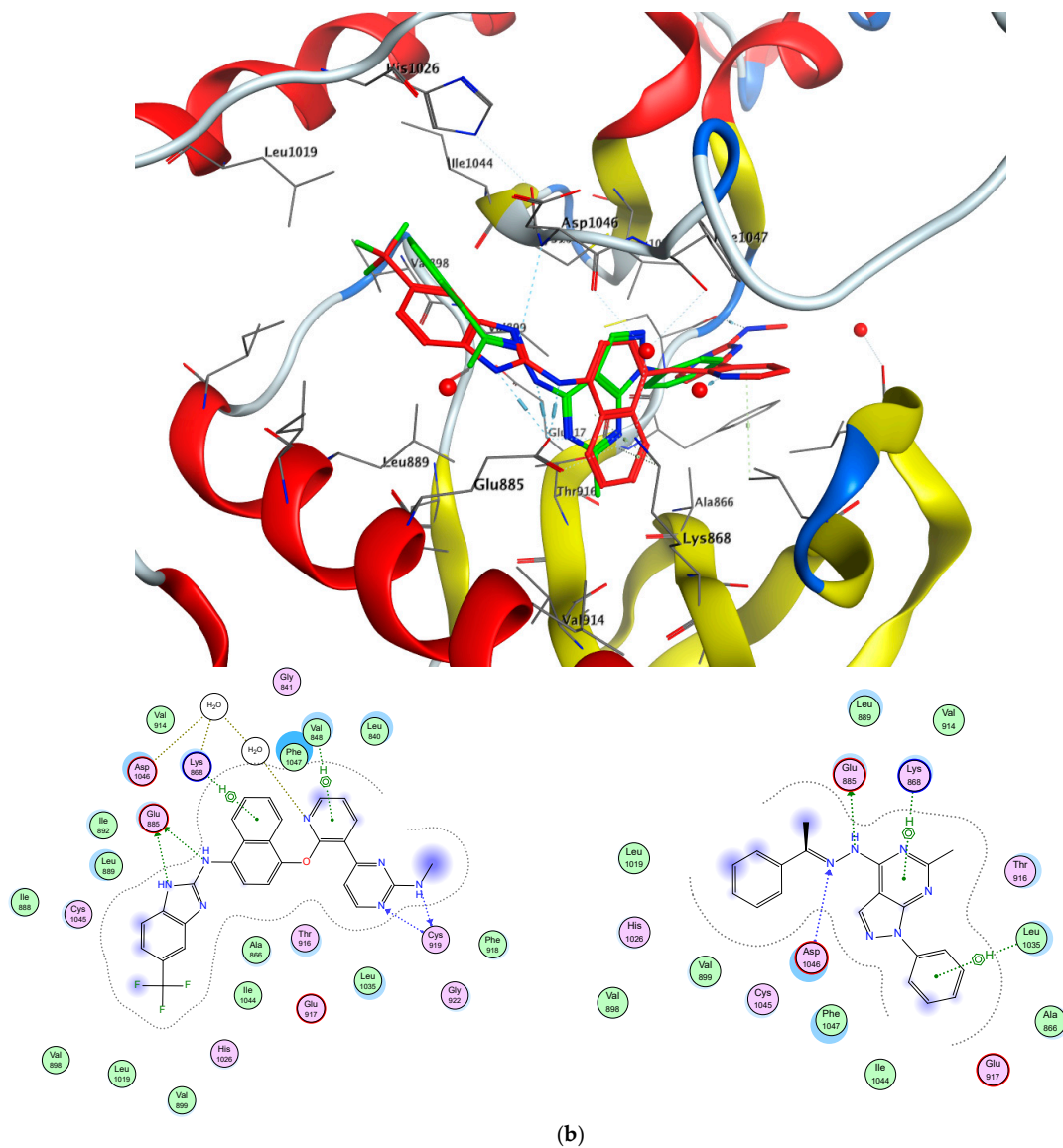


Figure 7. Docking modes of active compound **5i**. Shown are the predicted complexes of (a) an erlotinib drug with EGFR and (b) a pyridyl-pyrimidine benzimidazole derivative with VGFR.

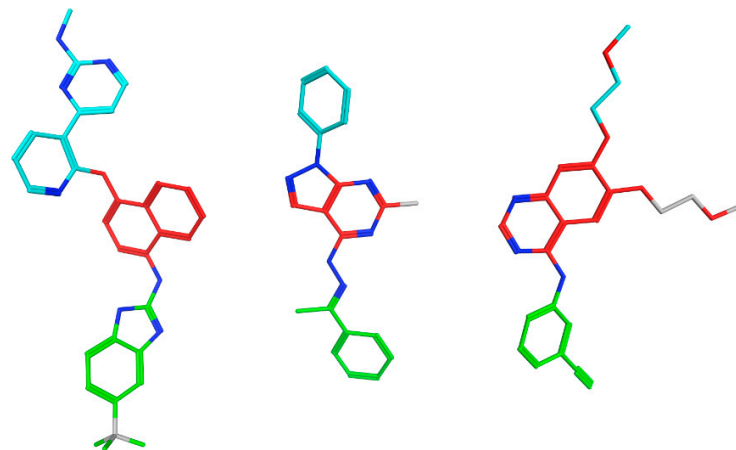


Figure 8. Molecular mapping of compound **5i** (middle) to reference bound ligands within protein targets. Color coding of similar fragments: red, green, and cyan types.

Table 4. Toxicity risks and physicochemical properties of compounds **5b** and **5i** in comparison with reported drugs, as predicted by the OSIRIS Property Explorer.

| ID | Molecular Properties | | | | Druggability | | Toxicity Risks | | | | %ABS |
|-----------|----------------------|-----|------------|-------|---------------|------------|----------------|---|------|---|-------|
| | TPSA | Mwt | Solubility | ClogP | Drug-likeness | Drug-Score | M | T | I | R | |
| 5b | 88.22 | 344 | −4.09 | 4.29 | 3.97 | 0.66 | | | Safe | | 78.56 |
| 5i | 67.99 | 342 | −4.74 | 4.57 | 4.26 | 0.58 | | | Safe | | 85.54 |
| Sorafenib | 92.35 | 464 | −6.69 | 4.14 | −4.2 | 0.2 | | | Safe | | 77.13 |
| Erlotinib | 74.73 | 393 | −3.53 | 3.07 | −6.73 | 0.38 | | | Safe | | 83.21 |

- <https://www.organic-chemistry.org/prog/peo> (accessed on 25 September 2023). The calculation of %ABS was conducted using this equation $ABS = 109 - (0.345 \times TPSA)$. Safe term indicates very low toxicity risks.

3. Conclusions

In this work, we applied a well-established chemical approach to the design and synthesis of phenylpyrazolopyrimidine-based analogs. In the protocol, we synthesized four different series of hydrazide, methylhydrazide, closed ring systems, and thiourea derivatives of high accessibility and good yields. The resulting compounds were evaluated for cytotoxic activity using an MTT assay against three malignant cell lines. Moreover, exemplary compounds were selected for mechanistic analysis using EGFR, VGFR-2, and Top-II enzymatic assay and cell cycle and apoptotic analyses. Most of the synthesized derivatives exhibited greater potency and selectivity performance than the reference inhibitor. Compounds **5b**, **5i**, and **9e** were the most potent analogs, with IC_{50} values of 3–10 μ M cytotoxicity. Moreover, a detailed mechanistic analysis on the cancer cell line revealed that when compared to the positive control medication, most of the compounds had stronger antiproliferative activity. In MCF-7 cancer cells, compound **5i** also enhanced apoptosis, produced cell cycle arrest at the G2/M phase, and caused DNA fragmentation. Molecule **5i** appears to offer a lot of potential as a novel multi pyrazolopyrimidine-based lead compound for the identification of new anticancer medicines that target EGFR/VGFR-2 enzymes, based on our findings. In future studies, we intend to keep optimizing this molecule to create chemical entities with great anticancer activity and better selectivity to be advanced to preclinical studies. We will also use this molecule as a starting point from which to develop a combination therapy.

4. Experimental Section

4.1. Chemistry

4.1.1. General Procedures

All solvents and reagents used in this work were utilized as received from suppliers unless otherwise noted. Melting points were determined on a StuartTM digital melting point apparatus (Stone, UK) and are uncorrected. The IR spectra were recorded on a Jasco FT/IR 460 plus spectrophotometer using KBr discs. The ¹H-NMR (400 MHz) and ¹³C-NMR (100 MHz) spectra were recorded on a Varian Mercury VXR-400 NMR 300 MHz using DMSO-*d*₆ as a solvent, and mass spectra were measured using a Hewlett Packard 5988 spectrometer. Elemental analysis was conducted at the Regional Centre for Mycology and Biotechnology (RCMP), Al-Azhar University, Cairo, Egypt. Reaction progress and purity of the synthesized molecules were monitored via thin-layer chromatography (TLC), utilizing Merck precoated silica gel 60 F₂₅₄ aluminum sheets. The reported yields refer to isolated compounds after purification. All spectral data are present in Supplementary Materials.

6-Methyl-1-phenyl-1,5-dihydro-4H-pyrazolo[3,4-*d*]pyrimidin-4-one (1)

Compound 1 was prepared according to the procedure in [60].

4-Chloro-6-methyl-1-phenyl-1H-pyrazolo[3,4-*d*]pyrimidine (2)

Compound 6 was prepared according to the procedure in [61].

4-Hydrazinyl-6-methyl-1-phenyl-1H-pyrazolo[3,4-*d*]pyrimidine (3)

A mixture of 4-chloro-6-methyl-1-phenyl-1H-pyrazolo[3,4-*d*]pyrimidine (2) (0.01 mol) and hydrazine hydrate (99%, 5 mL, 0.1 mol) was refluxed for 8 h. After cooling, the formed precipitate was filtered, washed with hot ethanol (95%, 3 mL), and crystallized from isopropanol to yield compound 3: yellow solid; yield 73%; m.p. 236–238 °C; IR (KBr) ν (cm⁻¹): 3444–3352 (NH₂), 3190 (NH), 1660 (C=N), 1560 (C=C); ¹H NMR (DMSO-*d*₆) δ ppm: 8.26 (d, 2H, *J* = 7.90 Hz, phenyl-H2, H6), 8.17 (s, 1H-Ar-H C3-H-pyrazol), 7.56–7.60 (m, 3H, phenyl-H3, H4, H5), 7.54 (s, 1H, NH, exchanged with D₂O), 4.73 (brs, 2H, NH₂, exchanged with D₂O), 2.42 (s, 3H, pyrimidine-CH₃); ¹³C NMR (DMSO-*d*₆) δ (ppm): 164.5, 158.06, 156.04, 148.00, 134.03, 129.03, 127.13, 126.02, 119.90, 103.30, 26.20, 24.50; MS (*m/z*): 240.27 (M⁺, 8.95%), 171 (100%); Anal. Calcd. for C₁₂H₁₂N₆ (242.27): C, 59.59; H, 5.03; N, 34.98%. Found: C, 60.11; H, 5.15; N, 34.99%.

General Procedure for the Synthesis of 4-(2-Arylidenehydrazinyl)-6-methyl-1-phenyl-1H-pyrazolo[3,4-*d*]pyrimidine (5a–l)

A mixture of hydrazinyl derivative (3) (0.01 mol), appropriate aromatic aldehydes (4a–h) (0.01 mol), appropriate aromatic acetophenones (4i–l) (0.01 mol), and a catalytic amount of glacial acetic acid (0.5 mL) was heated under reflux in absolute ethanol (20 mL) for 4 h. The precipitate that formed was filtered and crystallized from ethanol to give the title compounds. The physical and spectral data of compounds 5a–l were as follows:

4-(2-Benzylidenehydrazinyl)-6-methyl-1-phenyl-1H-pyrazolo[3,4-*d*]pyrimidine (5a)

White solid; yield 70%; m.p. 160–162 °C; IR (KBr) ν (cm⁻¹): 3377 (NH), 3058, 2782 (CH), 1600 (C=N), 1540 (C=C); ¹H NMR (DMSO-*d*₆) δ ppm: 8.61 (s, 1H, NH, exchanged with D₂O), 8.33 (s, 1H, -CH=N), 8.23 (d, 2H, *J* = 7.91 Hz, phenyl-H2, H6), 8.21 (s, 1H-Ar-H C3-H-pyrazol), 8.07 (d, 2H, *J* = 7.91 Hz, phenyl-CH-H2, H), 7.85–7.61 (m, 3H, phenyl-CH-H3, H4, H5), 7.59–7.51 (m, 3H, phenyl-H3, H4, H5), 2.51 (s, 3H, pyrimidine-CH₃). ¹³C NMR (DMSO-*d*₆) δ (ppm): 164.81, 155.96, 146.93, 139.24, 137.40, 134.46, 130.54, 129.64, 127.52, 126.79, 122.53, 121.48, 99.37, 40.60, 39.35, 25.83; MS (*m/z* (%)): 328 (M⁺, 10.26); Anal. Calcd for C₁₉H₁₆N₆ (328.37): C, 69.50; H, 4.91; N, 25.59%. Found: C, 69.23; H, 4.95; N, 25.48%.

4-((2-(6-Methyl-1-phenyl-1H-pyrazolo[3,4-*d*]pyrimidin-4-yl)hydrazineylidene)methyl)phenol (5b)

White solid; yield 75%; m.p. 162–164 °C; IR (KBr) ν (cm⁻¹): 3505 (br, OH), 3294 (NH), 3150 (CH aromatic), 1632 (C=N); ¹H NMR (DMSO-*d*₆) δ ppm: 10.79 (s, 1H, NH, exchanged with D₂O), 9.89 (s, 1H, OH, exchanged with D₂O), 8.60 (s, 1H, -CH=N), 8.20 (d, 2H, *J* = 7.91 Hz, phenyl-H2, H6), 8.18 (s, 1H-Ar-H C3-H-pyrazol), 8.05 (d, 2H, *J* = 7.91 Hz, phenyl-CH-H2, H), 7.89–7.68 (m, 2H, phenyl-H4, H5), 7.68–7.63 (m, 3H, phenyl-H3, H4, H5), 2.51 (s, 3H, pyrimidine-CH₃). ¹³C NMR (DMSO-*d*₆) δ (ppm): 163.25, 161.53, 160.28, 158.39, 154.05, 151.01, 146.64, 137.81, 136.83, 131.24, 129.86, 127.11, 125.09, 122.56, 116.29, 98.53, 39.23, 23.06; MS (*m/z* (%)): 344 (M⁺, 11.55); Anal. Calcd for C₁₉H₁₆N₆O (344.37): C, 66.27; H, 4.68; N, 24.40%. Found: C, 65.98; H, 4.84; N, 24.61%; purity via HPLC = 98.23%.

4-(2-(4-Chlorobenzylidene)hydrazinyl)-6-methyl-1-phenyl-1H-pyrazolo[3,4-*d*]pyrimidine (5c)

White solid; yield 79%; m.p. 233–235 °C; IR (KBr) ν (cm⁻¹): 3450 (NH), 3002, 2917 (CH), 1580 (C=N); ¹H NMR (DMSO-*d*₆) δ ppm: 11.7 (s, 1H, NH, exchanged with D₂O), 8.58 (s, 1H, -CH=N), 8.25 (d, 2H, *J* = 7.91 Hz, phenyl-H2, H6), 8.24 (s, 1H, Ar-H C3-H-pyrazol), 8.23 (d, 2H, *J* = 7.91 Hz, phenyl-CH-H2, H), 7.86–7.84 (m, 3H, phenyl-CH-H3, H4, H5), 7.59–7.54 (m, 2H, phenyl-H4, H5), 2.51 (s, 3H, pyrimidine-CH₃). ¹³C NMR (DMSO-*d*₆) δ (ppm): 167.90, 166.02, 160.28, 158.39, 154.05, 151.01, 146.64, 137.81, 136.83, 130.06, 129.86, 127.11, 125.09, 122.56, 119.29, 98.53, 39.23, 24.04; MS (*m/z*): 364 (M⁺+2, 10.3), 362 (M⁺, 32.0); Anal. Calcd for C₁₉H₁₅ClN₆ (362.82): C, 62.90; H, 4.17; N, 23.16%. Found: C, 62.71; H, 4.19; N, 23.22%.

4-(2-(4-Methoxybenzylidene)hydrazineyl)-6-methyl-1-phenyl-1H-pyrazolo[3,4-*d*]pyrimidine (5d)

Green solid; yield 90%; m.p. 227–229 °C; IR (KBr) ν (cm⁻¹): 3418 (NH), 3054 (Ar-H), 2932 (aliph-CH), 1542 (C=N); ¹H NMR (DMSO-*d*₆) δ ppm: 8.94 (s, 1H, pyrimidine-NH), 8.74 (s, 1H, phenyl-CH=N, H1), 8.59 (d, 2H, *J* = 7.3 Hz, phenyl-H2, H6), 8.26 (s, 1H-pyrazol), 8.22 (d, 2H, *J* = 7.3 Hz, phenyl-C=N, H2, H6), 8.05–7.80 (m, 3H, phenyl-H3, H4, H5), 7.78 (d, 2H, *J* = 7.3 Hz, phenyl-H3, H5), 3.84 (s, 3H, phenyl-H5), 2.51 (s, 3H, pyrimidine-CH₃); ¹³C NMR (DMSO-*d*₆): 1641.41, 155.27, 154.57, 147.51, 139.04, 137.40, 131.04, 129.265, 129.90, 126.88, 122.56, 121.62, 99.49, 55.79, 25.50, 23.11; MS *m/z* (%): 358 (M⁺, 5.23); Anal. Calc. for C₂₀H₁₈N₆O (358.40): C, 67.02; H, 5.06; N, 23.45%. Found: C, 67.28; H, 5.08; N, 23.48%.

4-(2-(2-Methoxybenzylidene)hydrazineyl)-6-methyl-1-phenyl-1H-pyrazolo[3,4-*d*]pyrimidine (5e)

Brownish solid; yield 86%; m.p. 220–222 °C; IR (KBr) ν (cm⁻¹): 3412 (NH), 3076, 2955 (CH), 1550 (C=N); ¹H NMR (DMSO-*d*₆) δ ppm: 8.94 (s, 1H, pyrimidine-NH, H4), 8.74 (s, 1H, phenyl-CH=N, H1), 8.59 (d, 2H, *J* = 7.3 Hz, phenyl-H2, H6), 8.26 (s, 1H-pyrazol), 8.22(d, 2H, *J* = 7.3 Hz, phenyl-C=N, H2, H5), 8.05–7.80 (m, 3H, phenyl-H3, H4, H5), 7.78 (d, 2H, *J* = 7.3 Hz, phenyl-H3, H4), 3.84 (s, 3H, -OCH₃), 2.51 (s, 3H, pyrimidine-CH₃). ¹³C-NMR (DMSO-*d*₆): 163.09, 158.17, 154.39, 148.66, 146.66, 146.94, 143.71, 138.95, 137.47, 132.29, 129.90, 122.47, 121.61, 99.32, 25.27, 18.96.; MS (*m/z*): 358 (M⁺, 21.58); Anal. Calcd. for C₂₀H₁₈N₆O (358.40): C, 67.02; H, 5.06; N, 23.45%. Found: C, 67.28; H, 5.08; N, 23.48%.

6-Methyl-4-(2-(4-nitrobenzylidene)hydrazineyl)-1-phenyl-1H-pyrazolo[3,4-*d*]pyrimidine (5f)

Orange solid; yield 88%; m.p. 250–252 °C; IR (KBr) ν (cm⁻¹): 3305 (NH), 3057, 2975 (CH), 1510 (C=N); ¹H NMR (DMSO-*d*₆) δ ppm: 12.52 (s, 1H, pyrimidine-NH, H4), 8.64 (s, 1H, phenyl-CH=N, H1), 8.39 (d, 2H, *J* = 7.3, phenyl-CH=N, H2, H6), 8.37 (d, 2H, *J* = 7.3 Hz, phenyl-H2, H6), 8.23 (s, 1H-pyrazol), 8.18 (s, 2H, phenyl-H3, H5) 7.61–7.59 (m, 3H, phenyl-H3, H4, H4), 2.50 (s, 3H, pyrimidine-CH₃). ¹³C-NMR (DMSO-*d*₆): 147.86, 139.25, 125.99, 129.55, 128.14, 126.65, 124.54, 121.30, 40.45, 40.24, 40.03, 39.83, 39.62, 39.41, 39.20.; MS (*m/z*): 373 (M⁺, 24.32); Anal. Calcd for C₁₉H₁₅N₇O₂ (373.37): C, 61.12; H, 4.05; N, 26.26%. Found: C, 60.89; H, 4.06; N, 26.32%.

4-(2-(2,6-Dichlorobenzylidene)hydrazineyl)-6-methyl-1-phenyl-1H-pyrazolo[3,4-*d*]pyrimidine (5g)

Red solid; yield 83%; m.p. 255–257 °C; IR (KBr) ν (cm⁻¹): 3383 (NH), 3109, 2910 (CH), 1570 (C=N); ¹H NMR (DMSO-*d*₆) δ ppm: 8.55 (s, 1H, pyrimidine-NH), 8.39 (s, 1H, -CH=N, H1), 8.24 (d, 2H, *J* = 7.3 Hz, phenyl-H2, H6), 8.18 (s, 1H, -pyrazol), 7.65–7.60 (m, 3H, phenyl-H3, H4, H5), 7.39 (d, 2H, *J* = 7.3 Hz, phenyl-H3, H5), 7.38 (m, 1H, phenyl-H4), 2.33 (s, 3H, pyrimidine-CH₃). ¹³C-NMR (DMSO-*d*₆): 165.9, 156.1, 154.8, 141.4, 139.1, 136.6, 134.1, 131.1, 131.6, 130.2, 129.9, 126.8, 99.4, 25.9; MS (*m/z*): 400 (M⁺+4, 7.5), 398 (M⁺+2, 50.6), 396 (M⁺, 76.45); Anal. Calcd for C₁₉H₁₄Cl₂N₆ (397.26): C, 57.44; H, 3.55; N, 21.15%. Found: C, 57.42; H, 3.51; N, 21.21%.

6-Methyl-1-phenyl-4-(2-(3-phenylallylidene)hydrazineyl)-1H-pyrazolo[3,4-*d*]pyrimidine (5h)

Orange solid; yield 95%; m.p. 241–243 °C; IR (KBr) ν (cm⁻¹): 3317 (NH), 3112, 2886 (CH), 1550 (C=C), 1670 (C=N); ¹H NMR (DMSO-*d*₆) δ ppm: 10.46 (s, 1H, NH), 8.39 (d, 2H, *J* = 7.4 Hz, phenyl-H2, H6), 8.18 (s, 1H-pyrazol), 7.94 (s, 1H, N=CH), 7.60–7.52 (m, 3H, phenyl-H3, H4, H5), 7.54 (d, 2H, *J* = 7.4 Hz, phenyl-H2, H6), 7.45–7.33 (m, 3H, phenyl-H3, H4, H5), 7.22 (d, 1H, *J* = 7.5 Hz, CH=CH-ph), 6.89 (d, 1H, *J* = 12 Hz, N=CH-CH=CH), 2.35 (s, 3H, pyrimidine-CH₃). ¹³C-NMR (DMSO-*d*₆): 164.2, 155.3, 154.5, 149.3, 139.2, 139.1, 137.4, 136.4, 129.6, 127.6, 126.9, 125.1, 122.5, 99.5, 56.5, 25.5, 18.9.; MS (*m/z*): 354 (M⁺, 100); Anal. Calcd for C₂₁H₁₈N₆ (354.41): C, 71.17; H, 5.12; N, 23.71%. Found: C, 71.14; H, 5.18; N, 23.74%.

6-Methyl-1-phenyl-4-(2-(1-phenylethylidene)hydrazinyl)-1H-pyrazolo[3,4-*d*]pyrimidine (5i)

White solid; yield 90%; m.p. 245–247 °C; IR (KBr) ν (cm⁻¹): 3140 (NH), 3058, 2900 (CH), 1610 (C=N); ¹H NMR (DMSO-*d*₆) δ ppm: 11.52 (s, 1H, -NH), 8.52 (d, 2H, *J* = 7.3 Hz,

phenyl-H2, H6), 8.15 (s, 1H-pyrazol), 8.14 (d, 2H, $J = 7.3$ Hz, phenyl-C=N, H2, H6), 7.92–7.90 (m, 3H, phenyl-H3, H4, H5), 7.55–7.51 (m, 3H, phenyl-C=N, H3, H4, H5), 2.60 (s, 3H, CH₃-C=N-), 2.50 (s, 3H, pyrimidine-CH₃); ¹³C-NMR (DMSO, *d*₆): 160.06, 155.46, 153.52, 01, 138.53, 137.95, 136.72, 133.65, 130.35, 129.69, 128.58, 126.95, 121.89, 113.38, 99.41, 12.27, 15.19; MS (*m/z*): 342 (M⁺, 13.09); Anal. Calcd for C₂₀H₁₈N₆ (342.40): C, 70.16; H, 5.30; N, 24.54. Found: C, 69.83; H, 5.32; N, 24.58%, purity by HPLC = 98.20%.

4-(1-(2-(6-Methyl-1-phenyl-1H-pyrazolo[3,4-*d*]pyrimidin-4-yl)hydrazineylidene)ethyl)aniline (5j)

White solid; yield 86%; m.p. 221–223 °C; IR (KBr) ν (cm⁻¹): 3336, 3249 (NH₂), 3197 (NH), 3073, 2931 (CH), 1615 (C=N); ¹H NMR (DMSO-*d*₆) δ ppm: 10.13 (s, 1H, -NH, H4), 8.67 (d, 2H, $J = 7.3$ Hz, phenyl-H2, H6), 8.17 (s, 1H-pyrazol), 8.15 (d, 2H, $J = 7.3$ Hz, phenyl-C=N, H2, H6), 7.86–7.84 (m, 3H, -H3, H4, H5), 7.73–7.70 (m, 2H, phenyl-C=N, H3, H5), 3.36 (brs, 2H, -NH₂), 2.95 (s, 3H, CH₃-C=N-), 2.51 (s, 3H, pyrimidine-CH₃); ¹³C-NMR (DMSO, *d*₆): 167.9, 166.2, 164.13, 150.7, 149.87, 148.00, 140.22, 138.74, 133.49, 129.81, 127.76, 122.35, 102.83, 20.81, 17.00 14.73; MS (*m/z*): 357 (M⁺, 13.09); Anal. Calcd for C₂₀H₁₉N₇ (357.41): C, 67.21; H, 5.36; N, 27.43%. Found: C, 67.45; H, 5.38; N, 27.48%.

4-(2-(1-(4-Methoxyphenyl)ethylidene)hydrazinyl)-6-methyl-1-phenyl-1H-pyrazolo[3,4-*d*]pyrimidine (5k)

Yellowish solid; yield 85%; m.p. 235–237 °C; IR (KBr) ν (cm⁻¹): 3190 (NH), 3085, 2965 (CH), 1580 (C=N); ¹H NMR (DMSO-*d*₆) δ ppm: 10.12 (s, 1H, pyrimidine-NH, H4), 8.59 (d, 2H, $J = 7.3$ Hz, phenyl-H2, H6), 8.26 (s, 1H-pyrazol), 8.22 (d, 2H, $J = 7.3$ Hz, phenyl-C=N, H2, H6), 8.05–7.80 (m, 3H, phenyl-H3, H4, H5), 7.78 (d, 2H, $J = 7.3$ Hz, phenyl-C=N-, H3, H5), 3.84 (s, 3H, -OCH₃), 2.95 (s, 3H, CH₃-C=N-), 2.51 (s, 3H, pyrimidine-CH₃). ¹³C-NMR (DMSO, *d*₆): 167.9, 166.2, 155.59, 153.99, 151.89, 149.63, 141.78, 138.50, 135.09, 133.67, 129.72, 128.83, 125.20, 121.03, 105.67, 24.78, 17.47; MS (*m/z*): 372 (M⁺, 22.7); Anal. Calcd for C₂₁H₂₀N₆O (372.42): C, 67.73; H, 5.41; N, 22.57%. Found: C, 67.79; H, 5.43; N, 22.62%.

4-(2-(1-(2-Bromo-4-chlorophenyl)ethylidene)hydrazineyl)-6-methyl-1-phenyl-1H-pyrazolo[3,4-*d*]pyrimidine (5l)

Orange crystals; yield 75%; m.p. 257–259 °C; IR (KBr) ν (cm⁻¹): 3123 (NH), 3080, 2924 (CH), 1535 (C=N); ¹H NMR (DMSO-*d*₆) δ ppm: 10.12 (s, 1H, pyrimidine-NH, H4), 8.59 (d, 2H, $J = 7.3$ Hz, phenyl-H2, H6), 8.26 (s, 1H-pyrazol), 8.22 (d, 2H, $J = 7.3$ Hz, -C=N, H2, H6), 7.80–8.05 (m, 2H, phenyl-H4, H5), 7.78 (d, 2H, $J = 7.3$ Hz, phenyl-C=N-, H3, H5), 2.95 (s, 3H, CH₃-C=N-), 2.51 (s, 3H, -CH₃); ¹³C-NMR (DMSO, *d*₆): 158.14, 153.98, 151.88, 148.93, 137.50, 134.09, 132.67, 129.72, 127.81, 127.04, 124.67, 124.07, 122.44, 121.03, 115.77, 106.66, 17.78; MS (*m/z*): 418 (M⁺, 37.01); Anal. Calcd for C₂₀H₁₆BrClN₆ (455.74): C, 52.71; H, 3.54; N, 18.44%. Found: C, 52.97; H, 3.58; N, 18.52%.

General Procedure for the Synthesis of Pyrazolopyrimidine Derivatives (6a–d)

A mixture of hydrazinyl derivative (3) (0.01 mol) and carboxylic acid derivatives, namely, triethyl orthoformate, trifluoroacetic acid, and trichloroacetic acid or acetyl acetone/glacial acetic acid (0.01 mol/20 mL), was refluxed for 3–5 h. The reaction mixture was allowed to cool, leading to separation of the product, and then the crude product was filtered, dried, and crystallized from 1,4-dioxane to give 6a–c. The physical and spectral data of compounds 6a–d were as follows:

5-Methyl-7-phenyl-7H-pyrazolo[4,3-*e*][1,2,4]triazolo[4,3-*c*]pyrimidine (6a)

White solid; yield 74%; m.p. 250–252 °C; IR (KBr) ν (cm⁻¹): 3040, 2967 (CH), 1595 (C=C), 1648 (C=N); ¹H NMR (DMSO-*d*₆) δ ppm: 8.80 (s, 1H, Triazol-H2), 8.74 (d, 2H, $J = 7.90$ Hz, phenyl-H2, H6), 8.19 (s, 1H, -pyrazol), 7.65–7.61 (m, 3H, phenyl-H3, H4, H5), 2.51 (s, 3H, pyrimidine-CH₃); ¹³C-NMR (DMSO-*d*₆) δ ppm: 159.20, 144.81, 139.09, 138.74, 134.03, 131.93, 128.13, 123.7, 120.75, 117.71, 42.77; MS (*m/z*): 250.27 (C₁₃H₁₀N₆, 78.57%, M⁺); Anal. Calc. for: (C₁₃H₁₀N₆), C, 62.39; H, 4.03; N, 33.05%; Found: C, 62.15; H, 4.05; N, 33.69%.

5-Methyl-7-phenyl-3-(trifluoromethyl)-7H-pyrazolo[4,3-e][1,2,4]triazolo[4,3-c]pyrimidine (6b)

White crystals; yield 69%; m.p. 267–269 °C; IR (KBr) ν (cm⁻¹): 3027, 2933 (CH), 1596 (C=C), 1662 (C=N); ¹H-NMR (DMSO-*d*₆) δ ppm: 8.61 (d, 2H, *J* = 7.90 Hz, phenyl-H2, H6), 8.13 (s, 1H, H-pyrazol), 7.41–7.61 (m, 3H, phenyl-H3, H4, H5), 2.54 (s, 3H, pyrimidine-CH3); ¹³C-NMR (DMSO-*d*₆) δ ppm: 159.31, 144.81, 139.09, 138.74, 134.03, 131.93, 128.13, 123.96, 120.75, 120.39, 117.71, 42.77; MS (*m/z*): 318.26 (78.57%, M⁺); Anal. Calcd. for: (C₁₄H₉F₃N₆): C, 52.83; H, 2.85; N, 26.41%. Found: C, 53.03; H, 2.87; N, 26.32%.

5-Methyl-7-phenyl-3-(trichloromethyl)-7H-pyrazolo[4,3-e][1,2,4]triazolo[4,3-c]pyrimidine (6c)

Yellow solid; yield 74%; m.p. 250–252 °C; IR (KBr) ν (cm⁻¹): 3015, 2908 (CH), 1597 (C=C), 1685 (C=N); ¹H-NMR (DMSO-*d*₆) δ ppm: 8.67 (d, 2H, *J* = 7.90 Hz, phenyl-H2, H6), 8.16 (s, 1H, -pyrazol), 7.65–7.61 (m, 3H, phenyl-H3, H4, H5), 2.51 (s, 3H, pyrimidine-CH3); ¹³C-NMR (DMSO-*d*₆) δ ppm: 159.31, 144.81, 139.09, 138.74, 134.03, 131.93, 128.13, 123.96, 123.7, 120.75, 120.39, 117.71, 42.77; MS (*m/z*): 367.62 (78.57%, M⁺); Anal. Calcd. for: (C₁₄H₉Cl₃N₆): C, 45.74; H, 2.47; N, 22.86%; Found: C, 45.89; H, 2.46; N, 22.95%.

4-((6-Methyl-1-phenyl-1H-pyrazolo[3,4-*d*]pyrimidin-4-yl)imino)pentan-2-one (6d)

White solid; yield 69%; m.p. 240–242 °C; IR (KBr, ν , cm⁻¹): 3065 (CH-aromatic), 2982 (CH-aliphatic), 1655 (C=N), 1560 (C=C). ¹H-NMR (DMSO-*d*₆): δ ppm: 8.98 (d, 2H, *J* = 7.90 Hz, phenyl-H2, H6), 8.49 (s, 1H, -pyrazol), 7.58–7.54 (m, 3H, phenyl-H3, H4, H5), 6.10 (m, 3H), 4.15 (s, 2H, NH-CH2-), 2.51 (s, 3H, pyrimidine-CH3), 2.43 (s, 3H-pyrazol-(CH3)), ¹³C-NMR (DMSO): 156.59, 154.90, 152.82, 150.66, 140.96, 138.50, 135.57, 133.09, 129.79, 128.13, 127.41, 126.11, 124.07, 109.78, 13.24. MS (*m/z*): 307.15 (18.4%, M⁺); Anal. Calcd. for C₁₇H₁₇N₅O (307.15): C, 67.09; H, 5.30; N, 27.61%. Found: C, 67.12; H, 5.28; N, 26.63%.

General Procedure for the Synthesis of Pyrrole-2,5-Dione Derivatives (7,8)

To a solution of hydrazinyl derivative (**3**, 0.01 mol) in glacial acetic acid (20 mL), dihydrofuran-2,5-dione, furan-2,5-dione, and indoline-2,3-dione (0.01 mol) were added. The reaction was refluxed at optimum temperature for 16 h. After completion of the reaction mixture (as indicated by TLC), the mixture was concentrated in vacuo and allowed to cool down. The formed solid was filtered and crystallized from ethanol to produce target compounds **7–9**. The physical and spectral data of compounds **7–9** were as follows:

1-((6-Methyl-1-phenyl-1H-pyrazolo[3,4-*d*]pyrimidin-4-yl)amino)pyrrolidine-2,5-dione (7)

Blue solid; yield 72%; m.p. 280–282 °C; IR (KBr) ν (cm⁻¹): 3450 (NH), 3073, 2965 (CH), 1662 (2 C=O); ¹H-NMR (DMSO-*d*₆): δ ppm: 9.80 (s, 1H, NH, exchanged with D₂O), 8.26 (d, 2H, *J* = 7.90 Hz, phenyl-H2, H6), 8.18 (s, 1H, -pyrazol), 7.58–7.54 (m, 3H, phenyl-H3, H4, H5), 2.64 (t, 4H, *J* = 7.90 Hz, pyrrolidin-H3, H4), 2.51 (s, 3H, pyrimidine-CH3); ¹³C NMR (DMSO): 171.00, 168.4, 164.5, 148.00, 139.7, 134.4, 129.3, 126.2, 119.9, 103.03, 30.00, 24.5; MS (*m/z*): 322.33 (39.48%, M⁺); Anal. Calcd. For C₁₆H₁₄N₆O₂ (322.33): C, 59.62; H, 4.38; N, 26.07%. Found: C, 59.89; H, 4.40; N, 26.12%.

1-((6-Methyl-1-phenyl-1H-pyrazolo[3,4-*d*]pyrimidin-4-yl)amino)-1H-pyrrole-2,5-dione (8)

White solid; yield 76%; m.p. 289–290 °C; IR (KBr) ν (cm⁻¹): 3449 (NH), 3073, 2945 (CH), 1662 (2 C=O); ¹H NMR (DMSO-*d*₆): δ ppm: 9.80 (s, 1H, NH, exchanged with D₂O), 8.26 (d, 2H, *J* = 7.90 Hz, phenyl-H2, H6), 8.18 (s, 1H, -pyrazol), 7.82 (d, 2H, *J* = 7.92 Hz, pyrrole-H3, H4), 7.56–7.58 (m, 3H, phenyl-H3, H4, H5), 2.50 (s, 3H, pyrimidine-CH3). ¹³C-NMR (DMSO): 171.00, 168.4, 164.5, 148.00, 139.7, 134.4, 129.3, 126.2, 119.9, 103.03, 30.00, 24.5. MS (*m/z*): 320.31 (31.96%, M⁺); Anal. Calcd. for C₁₆H₁₂N₆O₂ (320.35): C, 60.00; H, 3.78; N, 26.24%. Found: C, 60.14; H, 3.76; N, 26.28%.

General Procedure for the Synthesis of N-alkyl/aryl-2-(6-methyl-1-phenyl-1H-pyrazolo[3,4-*d*]pyrimidin-4-yl)hydrazinecarbothioamides (9a–e)

To a solution of hydrazinyl derivative (**3**) (0.01 mol) in butanol (20 mL), appropriate isothiocyanates (0.01 mol), namely, ethyl isothiocyanate, propyl isothiocyanate, butyl

isocyanate, vinyl isothiocyanate, and phenyl isothiocyanate (0.01 mol), were added drop wise at 0 °C. The mixture was stirred for 7–10 h at room temperature. Then, the solvent was evaporated under vacuo. The crude product was crystallized from ethanol to afford the corresponding compounds **9a–e**, respectively. The physical and spectral data of compounds **9a–e** were as follows:

N-Ethyl-2-(6-methyl-1-phenyl-1H-pyrazolo[3,4-*d*]pyrimidin-4-yl)hydrazinecarbothioamide (9a)

Yellowish-white solid; yield 72%; m.p. 278–280 °C; IR (KBr) ν (cm⁻¹): 3292 (NH), 3079, 2972 (CH), 1520 (C=C), 1655 (N=C); ¹H-NMR (DMSO-*d*₆): δ ppm: 10.09 (s, 1H, NH-NH-C=S), 9.15 (s, 1H, NH-NH-C=S), 8.26 (d, 2H, *J* = 7.90 Hz, phenyl-H2, H6), 8.19 (s, 1H, -pyrazol), 7.59–7.58 (m, 3H, phenyl-H3, H4, H5), 7.30 (s, 1H, C=S-NH-CH2), 4.16 (q, 2H, *J* = 7.2 Hz, -CH2CH3), 2.38 (s, 3H, pyrimidine-CH3), 1.20 (t, 3H, *J* = 7.2, -CH2CH3); ¹³C NMR (DMSO,₆): 182.52, 168.4, 164.5, 148.00, 139.16, 134.50, 129.66, 126.78, 121.37, 103.3, 40.45, 26.25, 14.84. MS (*m/z*): 327.41 (13.99%, M⁺), 89.33 (100%); Anal. Calcd. for C₁₅H₁₇N₇S (327.41): C, 55.03; H, 5.23; N, 29.59%. Found: C, 55.24; H, 5.21; N, 29.83%.

2-(6-Methyl-1-phenyl-1H-pyrazolo[3,4-*d*]pyrimidin-4-yl)-N-propylhydrazinecarbothioamide (9b)

White solid; yield 74%; m.p. 280–282 °C; IR (KBr) ν (cm⁻¹): 3260 (NH), 3067, 2904 (CH), 1527 (C=C), 1658 (N=C); ¹H-NMR (DMSO-*d*₆): δ ppm: 9.98 (s, 1H, NH-NH-C=S), 9.84 (s, 1H, NH-NH-C=S), 8.21 (d, 2H, *J* = 7.90 Hz, phenyl-H2, H6), 8.19 (s, 1H, -pyrazol), 7.58–7.54 (m, 3H, phenyl-H3, H4, H5), 7.37 (s, 1H, C=S-NH-CH2), 3.33 (t, 2H, *J* = 7.2 Hz, NH-CH2-), 2.58 (m, 2H, *J* = 7.2 Hz, NH-CH2-CH3), 2.38 (s, 3H, pyrimidine-CH3), 1.04 (t, 3H, *J* = 6.9, -CH2CH3); ¹³C-NMR (DMSO,₆): 184.20, 168.40, 164.50, 148.00, 139.70, 134.30, 129.30, 126.20, 119.9, 103.30, 46.40, 24.50, 23.30, 11.80; MS (*m/z*): 341.44 (15.14%, M⁺); Anal. Calcd. For C₁₆H₁₉N₇S (341.44): C, 56.28; H, 5.61; N, 28.72%. Found: C, 56.50; H, 5.63; N, 28.75%.

N-Butyl-2-(6-methyl-1-phenyl-1H-pyrazolo[3,4-*d*]pyrimidin-4-yl)hydrazinecarbothioamide (9c)

Grayish crystals; yield 75%; m.p. 270–272 °C; IR (KBr) ν (cm⁻¹): 3320 (NH), 3080, 2970 (CH), 1527 (C=C), 1658 (N=C); ¹H-NMR (DMSO-*d*₆): δ ppm: 10.09 (s, 1H, NH-NH-C=S), 9.25 (s, 1H, NH-NH-C=S), 8.36 (d, 2H, *J* = 7.90 Hz, phenyl-H2, H6), 8.28 (s, 1H, -pyrazol), 7.60–7.58 (m, 3H, phenyl-H3, H4, H5), 7.32 (s, 1H, C=S-NH-CH2), 4.13 (t, 2H, *J* = 7.2 Hz, NH-CH2CH2), 2.51 (s, 3H, pyrimidine-CH3), 1.30 (m, 2H, NH-CH2CH2), 1.17 (q, 2H, CH2-CH2-CH2CH3), 0.89 (t, 3H, *J* = 7.2 Hz, -CH2CH2-CH2CH3); ¹³C-NMR (DMSO,₆): 184.20, 168.40, 164.50, 148.00, 139.70, 134.30, 129.30, 126.20, 119.9, 103.30, 46.40, 32.40, 24.50, 20.30, 20.40; MS (*m/z*): 341.44 (15.14%, M⁺), Anal. Calcd. for C₁₇H₂₁N₇S (355.46): C, 57.44; H, 5.96; N, 27.58%. Found: C, 57.70; H, 5.98; N, 27.60%.

2-(6-Methyl-1-phenyl-1H-pyrazolo[3,4-*d*]pyrimidin-4-yl)-N-vinylhydrazine-1-carbothioamide (9d)

White solid; yield 70%; m.p. 268–270 °C; IR (KBr) ν (cm⁻¹): 3356 (NH), 3081, 2908 (CH), 1570 (C=C), 1620 (C=N); ¹H-NMR (DMSO-*d*₆): δ ppm: 10.20 (s, 1H, NH-NH-C=S-NH), 8.30 (d, 2H, *J* = 7.90 Hz, phenyl-H2, H6), 8.17 (s, 1H, -pyrazol), 8.10 (d, 1H, *J* = 7.90 Hz, NH-NH-C=S), 7.82 (t, 1H, *J* = 7.90 Hz, S=C-NH-CH2-), 7.58–7.56 (m, 3H, phenyl-H3, H4, H5), 6.80 (m, 1H, *J* = 7.30, NH-CH2-CH=CH2), 6.10 (t, 1H, *J* = 7.2, C=S-NH-CH2=CH), 5.85 (d, 1H, *J* = 7.2 Hz, C=S-NHCH2-CH=CH), 2.48 (s, 3H, pyrimidine-CH3). ¹³C-NMR (DMSO): 184.22, 168.42, 164.52, 148.00, 141.00, 139.76, 134.32, 129.30, 126.22, 119, 93.3, 46.40, 24.50, 20.30.

2-(6-Methyl-1-phenyl-1H-pyrazolo[3,4-*d*]pyrimidin-4-yl)-N-phenylhydrazinecarbothioamide (9e)

Brown solid; yield 66%; m.p. 281–282 °C; IR (KBr) ν (cm⁻¹): 3265 (NH), 3026 (aromatic-CH), 2924 (aliphatic-CH), 1510 (C=C), 1530 (C=N); ¹H-NMR (DMSO-*d*₆): δ ppm: 10.13 (s,

1H, S=C-NH), 9.81 (s, 1H, -NH-S=C-NH), 9.13 (s, 1H, NH-NH-S=C), 8.98 (d, 2H, $J = 7.90$ Hz, phenyl-H2, H6), 8.49 (s, 1H, -pyrazol), 7.70 (d, 2H, $J = 7.90$ Hz, -NH-phenyl-H2, H6), 7.58–7.54 (m, 3H, phenyl-H3, H4, H5), 7.49–7.36 (m, 3H, NH-phenyl-H3, H4, H5), 2.51 (s, 3H, pyrimidine-CH3). ^{13}C -NMR (DMSO): 161.22, 156.03, 139.95, 139.30, 134.98, 129.61, 129.68, 129.12, 126.67, 122.67, 121.40, 98.97, 40.55, 40.35, 39.93, 39.51, 26.33. MS (m/z): 375.45 (M^+ , 13.70%), Anal. Calcd. for $\text{C}_{19}\text{H}_{17}\text{N}_7\text{S}$ (375.45): C, 60.78; H, 4.56; N, 26.11%; Found: C, 61.05; H, 4.73; N, 26.16%, purity by HPLC = 98.84%.

4.2. Biological Evaluation

4.2.1. Cytotoxicity Evaluation Using Viability Assay

The cytotoxic activity was assessed using the 3-(4,5-dimethylthiazol-2-yl)-2,5-diphenyl tetrazolium bromide (MTT) colorimetric assay, as reported previously [62,63]. Doxorubicin was used as a reference standard, and DMSO was used as a negative control. Briefly, the designated cell lines were cultured at a concentration of 5×10^4 cell/well in 96-well plates. The cells were incubated for 24 h under optimum conditions. Following this, the designated molecules were introduced (in serial dilutions from 0 to 50 $\mu\text{g}/\text{mL}$), and the cells were incubated for an additional 24 h. Following this, the media were withdrawn, and 100 μL of fresh medium was added. Then, 10 μL of the 12 mM MTT stock solution was administered to each well. The plates were then incubated for 4 h. Then, the cells were exposed to different compounds at the desired concentrations (0.01, 0.1, 1, 10, and 100 μM) or to 1% dimethyl sulfoxide (DMSO) for 48 and 72 h. An 85- μL aliquot of the media was removed from the wells, and 50 μL of DMSO was added to each well and mixed thoroughly with the pipette and incubated at 37 $^\circ\text{C}$ for 10 min. Then, the optical density was measured at 590 nm with the microplate reader (Sunrise, TECAN, Inc., Morrisville, NC, USA).

4.2.2. In Vitro Enzyme Inhibitory Assays (against EGFR^{wt}, EGFR^{T790M}, VEGFR-2, and Topo II)

Enzyme inhibitory assays for the designated compounds **5b**, **5i**, and **9e** were carried out in triplicate, as described earlier [64]. The assays were conducted in Vacsera (Giza, Egypt). Curve fitting was performed using GraphPad Prism. Data are represented as means \pm SD from three independent experiments.

4.2.3. Quantification of Apoptosis by Flow Cytometry

Annexin V-FITC apoptosis assay was conducted utilizing the Annexin V-FITC/PI double staining detection kit (BD Pharmingen, San Diego, CA, USA), as described elsewhere [65,66].

4.2.4. Cell Cycle Analysis

Cell cycle arrest and distribution was evaluated using the Propidium Iodide Flow Cytometry Kit followed by flow cytometry analysis, as described previously [67].

4.3. Molecular Docking

The crystal structures of EGFR (PDB ID: 1M17) and VEGFR-2 (PDB ID: 3EWH) were extracted from Protein Data Bank (<http://www.pdb.org> (accessed on 25 September 2023)). The AutoDock 3.0 [68] and the MOE software 2008 [69] were used to perform all calculations on compound **5i**. The protocol in detailed [34] was adopted.

Supplementary Materials: The following supporting information can be downloaded at: <https://www.mdpi.com/article/10.3390/ijms241915026/s1>.

Author Contributions: A.K.B.A., W.A.Z.E.Z. and M.A. (Mohamed Alswah) conceived and designed the experiments; A.H., M.A.S., H.E.A.A., M.M.E. and A.H.B. performed the experiments; H.E.A.A., W.A.Z.E.Z., M.A. (Mohammad Almalghrabi), A.A.A. and M.A.S. implemented the biological study. H.E.A.A., M.M.E., A.M.E.-M. and M.A. (Marwa Alsulaimany) conducted all surface molecular modeling and contributed to the docking experiments' analysis. A.A.A. conducted the biological anticancer part and contributed to writing biological section. All authors analyzed the data, wrote the

paper, conducted English language editing, discussed the results, and commented on the manuscript. All authors have read and agreed to the published version of the manuscript.

Funding: The authors extend their appreciation to the Deputyship for Research and Innovation, Ministry of Education, Saudi Arabia, for funding this research work through project no. 445-9-238.

Institutional Review Board Statement: Not applicable.

Informed Consent Statement: Not applicable.

Data Availability Statement: All data are provided in the article or Supplementary Materials.

Conflicts of Interest: The authors declare that they have no known competing financial interest or personal relationships that could have appeared to influence the work reported in this paper.

References

1. Sener, S.F.; Grey, N. The global burden of cancer. *J. Surg. Oncol.* **2005**, *92*, 1–3. [[CrossRef](#)] [[PubMed](#)]
2. Salminen, E.; Iżewska, J.; Andreo, P. IAEA's role in the global management of cancer-focus on upgrading radiotherapy services. *Acta Oncol.* **2005**, *44*, 816–824. [[CrossRef](#)] [[PubMed](#)]
3. Rossari, F.; Zucchini, C.; Buda, G.; Orciuolo, E. Tumor dormancy as an alternative step in the development of chemoresistance and metastasis—Clinical implications. *Cell. Oncol.* **2020**, *43*, 155–176. [[CrossRef](#)] [[PubMed](#)]
4. El Azab, I.H.; Bakr, R.B.; Elkanzi, N.A.A. Facile One-Pot Multicomponent Synthesis of Pyrazolo-Thiazole Substituted Pyridines with Potential Anti-Proliferative Activity: Synthesis, In Vitro and In Silico Studies. *Molecules* **2021**, *26*, 3103. [[CrossRef](#)]
5. Omar, A.M.; Bajorath, J.; Ihmaid, S.; Mohamed, H.M.; El-Agrody, A.M.; Mora, A.; El-Araby, M.E.; Ahmed, H.E.A. Novel molecular discovery of promising amidine-based thiazole analogues as potent dual Matrix Metalloproteinase-2 and 9 inhibitors: Anticancer activity data with prominent cell cycle arrest and DNA fragmentation analysis effects. *Bioorganic Chem.* **2020**, *101*, 103992. [[CrossRef](#)]
6. Garraway, L.A.; Janne, P.A. Circumventing cancer drug resistance in the era of personalized medicine. *Cancer Discov.* **2012**, *2*, 214–226. [[CrossRef](#)]
7. Konstantinopoulos, P.A.; Papavassiliou, A.G. Seeing the future of cancer-associated transcription factor drug targets. *JAMA* **2011**, *305*, 2349–2350. [[CrossRef](#)] [[PubMed](#)]
8. Chohan, T.A.; Qayyum, A.; Rehman, K.; Tariq, M.; Akash, M.S.H. An insight into the emerging role of cyclin-dependent kinase inhibitors as potential therapeutic agents for the treatment of advanced cancers. *Biomed. Pharmacother.* **2018**, *107*, 1326–1341. [[CrossRef](#)] [[PubMed](#)]
9. Walker, S.R.; Xiang, M.; Frank, D.A. Distinct roles of STAT3 and STAT5 in the pathogenesis and targeted therapy of breast cancer. *Mol. Cell. Endocrinol.* **2014**, *382*, 616–621. [[CrossRef](#)]
10. Jackson, S.P.; Bartek, J. The DNA-damage response in human biology and disease. *Nature* **2009**, *461*, 1071–1078. [[CrossRef](#)]
11. Li, X.; Li, Z.; Wu, X.; Xiong, Z.; Yang, T.; Fu, Z.; Liu, X.; Tan, X.; Zhong, F.; Wan, X.; et al. Deep Learning Enhancing Kinome-Wide Polypharmacology Profiling: Model Construction and Experiment Validation. *J. Med. Chem.* **2020**, *63*, 8723–8737. [[CrossRef](#)] [[PubMed](#)]
12. Nassar, I.F.; Abdel Aal, M.T.; El-Sayed, W.A.; Shahin, M.A.E.; Elsakka, E.G.E.; Mokhtar, M.M.; Hegazy, M.; Hagra, M.; Mandour, A.A.; Ismail, N.S.M. Discovery of pyrazolo[3,4-d]pyrimidine and pyrazolo[4,3-e][1,2,4]triazolo[1,5-c]pyrimidine derivatives as novel CDK2 inhibitors: Synthesis, biological and molecular modeling investigations. *RSC Adv.* **2022**, *12*, 14865–14882. [[CrossRef](#)] [[PubMed](#)]
13. Abdelgawad, M.A.; Elkanzi, N.A.A.; Nayl, A.A.; Musa, A.; Alotaibi, N.H.; Arafa, W.A.A.; Gomha, S.M.; Bakr, R.B. Targeting tumor cells with pyrazolo[3,4-d]pyrimidine scaffold: A literature review on synthetic approaches, structure activity relationship, structural and target-based mechanisms. *Arab. J. Chem.* **2022**, *15*, 103781. [[CrossRef](#)]
14. Almeahadi, S.J.; Alsaedi, A.M.R.; Harras, M.F.; Farghaly, T.A. Synthesis of a new series of pyrazolo[1,5-a]pyrimidines as CDK2 inhibitors and anti-leukemia. *Bioorganic Chem.* **2021**, *117*, 105431. [[CrossRef](#)] [[PubMed](#)]
15. Chauhan, M.; Kumar, R. Medicinal attributes of pyrazolo[3,4-d]pyrimidines: A review. *Bioorganic Med. Chem.* **2013**, *21*, 5657–5668. [[CrossRef](#)] [[PubMed](#)]
16. Schenone, S.; Radi, M.; Musumeci, F.; Brullo, C.; Botta, M. Biologically Driven Synthesis of Pyrazolo[3,4-d]pyrimidines As Protein Kinase Inhibitors: An Old Scaffold As a New Tool for Medicinal Chemistry and Chemical Biology Studies. *Chem. Rev.* **2014**, *114*, 7189–7238. [[CrossRef](#)]
17. Hussein, E.M. Synthesis, cytotoxicity of some pyrazoles and pyrazolo[1,5-a]pyrimidines bearing benzothiazole moiety and investigation of their mechanism of action. *Bioorganic Chem.* **2020**, *102*, 104053. [[CrossRef](#)]
18. Abdellatif, K.R.A.; Bakr, R.B. Pyrimidine and fused pyrimidine derivatives as promising protein kinase inhibitors for cancer treatment. *Med. Chem. Res.* **2021**, *30*, 31–49. [[CrossRef](#)]
19. Cherukupalli, S.; Chandrasekaran, B.; Aleti, R.R.; Sayyad, N.; Hampannavar, G.A.; Merugu, S.R.; Rachamalla, H.R.; Banerjee, R.; Karpoornath, R. Synthesis of 4,6-disubstituted pyrazolo[3,4-d]pyrimidine analogues: Cyclin-dependent kinase 2 (CDK2) inhibition, molecular docking and anticancer evaluation. *J. Mol. Struct.* **2019**, *1176*, 538–551. [[CrossRef](#)]

20. Rahmouni, A.; Souiei, S.; Belkacem, M.A.; Romdhane, A.; Bouajila, J.; Ben Jannet, H. Synthesis and biological evaluation of novel pyrazolopyrimidines derivatives as anticancer and anti-5-lipoxygenase agents. *Bioorganic Chem.* **2016**, *66*, 160–168. [[CrossRef](#)] [[PubMed](#)]
21. Tabernero, J. The Role of VEGF and EGFR Inhibition: Implications for Combining Anti-VEGF and Anti-EGFR Agents. *Mol. Cancer Res.* **2007**, *5*, 203–220. [[CrossRef](#)]
22. Le, X.; Nilsson, M.; Goldman, J.; Reck, M.; Nakagawa, K.; Kato, T.; Ares, L.P.; Frimodt-Moller, B.; Wolff, K.; Visseren-Grul, C.; et al. Dual EGFR-VEGF Pathway Inhibition: A Promising Strategy for Patients With EGFR-Mutant NSCLC. *J. Thorac. Oncol.* **2021**, *16*, 205–215. [[CrossRef](#)] [[PubMed](#)]
23. Alblewi, F.F.; Okasha, R.M.; Eskandrani, A.A.; Afifi, T.H.; Mohamed, H.M.; Halawa, A.H.; Fouda, A.M.; Al-Dies, A.M.; Mora, A.; El-Agrody, A.M. Design and Synthesis of Novel Heterocyclic-Based 4H-benzo[h]chromene Moieties: Targeting Antitumor Caspase 3/7 Activities and Cell Cycle Analysis. *Molecules* **2019**, *24*, 1060. [[CrossRef](#)] [[PubMed](#)]
24. Alswah, M.; Bayoumi, A.H.; Elgamal, K.; Elmorsy, A.; Ihmaid, S.; Ahmed, H.E.J.M. Design, synthesis and cytotoxic evaluation of novel chalcone derivatives bearing triazolo [4, 3-a]-quinoxaline moieties as potent anticancer agents with dual EGFR kinase and tubulin polymerization inhibitory effects. *Molecules* **2018**, *23*, 48. [[CrossRef](#)] [[PubMed](#)]
25. Ihmaid, S.; Ahmed, H.E.A.; Zayed, M.F. The design and development of potent small molecules as anticancer agents targeting EGFR TK and tubulin polymerization. *Int. J. Mol. Sci.* **2018**, *19*, 408. [[CrossRef](#)] [[PubMed](#)]
26. Omar, A.M.; Ihmaid, S.; Habib, E.-S.E.; Althagfan, S.S.; Ahmed, S.; Abulkhair, H.S.; Ahmed, H.E. The Rational Design, Synthesis, and Antimicrobial Investigation of 2-Amino-4-Methylthiazole Analogues Inhibitors of GlcN-6-P Synthase. *Bioorganic Chem.* **2020**, *99*, 103781. [[CrossRef](#)] [[PubMed](#)]
27. Gossage, L.; Eisen, T. Targeting multiple kinase pathways: A change in paradigm. *Clin. Cancer Res. Off. J. Am. Assoc. Cancer Res.* **2010**, *16*, 1973–1978. [[CrossRef](#)]
28. Herbst, R.S.; Johnson, D.H.; Mininberg, E.; Carbone, D.P.; Henderson, T.; Kim, E.S.; Blumenschein, G., Jr.; Lee, J.J.; Liu, D.D.; Truong, M.T.; et al. Phase I/II trial evaluating the anti-vascular endothelial growth factor monoclonal antibody bevacizumab in combination with the HER-1/epidermal growth factor receptor tyrosine kinase inhibitor erlotinib for patients with recurrent non-small-cell lung cancer. *J. Clin. Oncol. Off. J. Am. Soc. Clin. Oncol.* **2005**, *23*, 2544–2555.
29. Fox, J.L.; MacFarlane, M. Targeting cell death signalling in cancer: Minimising 'Collateral damage'. *Br. J. Cancer* **2016**, *115*, 5–11. [[CrossRef](#)] [[PubMed](#)]
30. Fox, S.B.; Gasparini, G.; Harris, A.L. Angiogenesis: Pathological, prognostic, and growth-factor pathways and their link to trial design and anticancer drugs. *Lancet. Oncol.* **2001**, *2*, 278–289. [[CrossRef](#)]
31. Ellis, L.M. Epidermal growth factor receptor in tumor angiogenesis. *Hematol./Oncol. Clin. North Am.* **2004**, *18*, 1007–1021. [[CrossRef](#)] [[PubMed](#)]
32. Ahmed, H.E.; El-Nassag, M.A.; Hassan, A.H.; Mohamed, H.M.; Halawa, A.H.; Okasha, R.M.; Ihmaid, S.; El-Gilil, S.M.A.; Khattab, E.S.; Fouda, A.M.; et al. Developing lipophilic aromatic halogenated fused systems with specific ring orientations, leading to potent anticancer analogs and targeting the c-Src Kinase enzyme. *J. Mol. Struct.* **2019**, *1186*, 212–223. [[CrossRef](#)]
33. Ahmed, H.E.A.; El-Nassag, M.A.A.; Hassan, A.H.; Okasha, R.M.; Ihmaid, S.; Fouda, A.M.; Afifi, T.H.; Aljuhani, A.; El-Agrody, A.M. Introducing novel potent anticancer agents of 1H-benzo [f] chromene scaffolds, targeting c-Src kinase enzyme with MDA-MB-231 cell line anti-invasion effect. *J. Enzym. Inhib. Med. Chem.* **2018**, *33*, 1074–1088. [[CrossRef](#)] [[PubMed](#)]
34. Ahmed, H.E.A.; Ihmaid, S.K.; Omar, A.M.; Shehata, A.M.; Rateb, H.S.; Zayed, M.F.; Ahmed, S.; Elaasser, M.M. Design, synthesis, molecular docking of new lipophilic acetamide derivatives affording potential anticancer and antimicrobial agents. *Bioorganic Chem.* **2018**, *76*, 332–342. [[CrossRef](#)] [[PubMed](#)]
35. El-Moghazy, S.M.; George, R.F.; Osman, E.E.A.; Elbatrawy, A.A.; Kissova, M.; Colombo, A.; Crespan, E.; Maga, G. Novel pyrazolo[3,4-d]pyrimidines as dual Src-Abl inhibitors active against mutant form of Abl and the leukemia K-562 cell line. *Eur. J. Med. Chem.* **2016**, *123*, 1–13. [[CrossRef](#)] [[PubMed](#)]
36. Fraser, C.; Dawson, J.C.; Dowling, R.; Houston, D.R.; Weiss, J.T.; Munro, A.F.; Muir, M.; Harrington, L.; Webster, S.P.; Frame, M.C.; et al. Rapid Discovery and Structure–Activity Relationships of Pyrazolopyrimidines That Potently Suppress Breast Cancer Cell Growth via SRC Kinase Inhibition with Exceptional Selectivity over ABL Kinase. *J. Med. Chem.* **2016**, *59*, 4697–4710. [[CrossRef](#)]
37. Traxler, P.; Bold, G.; Frei, J.; Lang, M.; Lydon, N.; Mett, H.; Buchdunger, E.; Meyer, T.; Mueller, M.; Furet, P. Use of a pharmacophore model for the design of EGF-R tyrosine kinase inhibitors: 4-(phenylamino)pyrazolo[3,4-d]pyrimidines. *J. Med. Chem.* **1997**, *40*, 3601–3616. [[CrossRef](#)]
38. Ducray, R.; Ballard, P.; Barlaam, B.C.; Hickinson, M.D.; Kettle, J.G.; Ogilvie, D.J.; Trigwell, C.B. Novel 3-alkoxy-1H-pyrazolo[3,4-d]pyrimidines as EGFR and erbB2 receptor tyrosine kinase inhibitors. *Bioorganic Med. Chem. Lett.* **2008**, *18*, 959–962. [[CrossRef](#)]
39. Abdelgawad, M.A.; Bakr, R.B.; Alkhoja, O.A.; Mohamed, W.R. Design, synthesis and antitumor activity of novel pyrazolo[3,4-d]pyrimidine derivatives as EGFR-TK inhibitors. *Bioorganic Chem.* **2016**, *66*, 88–96. [[CrossRef](#)]
40. Elshaier, Y.A.M.M.; Shaaban, M.A.; Abd El Hamid, M.K.; Abdelrahman, M.H.; Abou-Salim, M.A.; Elgazwi, S.M.; Halaweish, F. Design and synthesis of pyrazolo[3,4-d]pyrimidines: Nitric oxide releasing compounds targeting hepatocellular carcinoma. *Bioorganic Med. Chem.* **2017**, *25*, 2956–2970. [[CrossRef](#)]
41. Cohen, S. Epidermal growth factor. *Vitr. Cell. Dev. Biol.* **1987**, *23*, 239–246. [[CrossRef](#)] [[PubMed](#)]

42. Nasser, A.A.; Eissa, I.H.; Oun, M.R.; El-Zahabi, M.A.; Taghour, M.S.; Belal, A.; Saleh, A.M.; Mehany, A.B.; Luesch, H.; Mostafa, A.E. Discovery of new pyrimidine-5-carbonitrile derivatives as anticancer agents targeting EGFR WT and EGFR T790M. *Org. Biomol. Chem.* **2020**, *18*, 7608–7634. [[CrossRef](#)] [[PubMed](#)]
43. Traxler, P.; Furet, P. Strategies toward the design of novel and selective protein tyrosine kinase inhibitors. *Pharmacol. Ther.* **1999**, *82*, 195–206. [[CrossRef](#)] [[PubMed](#)]
44. Sharma, V.K.; Nandekar, P.P.; Sangamwar, A.; Pérez-Sánchez, H.; Agarwal, S.M. Structure guided design and binding analysis of EGFR inhibiting analogues of erlotinib and AEE788 using ensemble docking, molecular dynamics and MM-GBSA. *RSC Adv.* **2016**, *6*, 65725–65735. [[CrossRef](#)]
45. Zhang, J.; Yang, P.L.; Gray, N.S. Targeting cancer with small molecule kinase inhibitors. *Nat. Rev. Cancer* **2009**, *9*, 28–39. [[CrossRef](#)]
46. Rezki, N.; Almeahadi, M.A.; Ihmaid, S.; Shehata, A.M.; Omar, A.M.; Ahmed, H.E.; Aouad, M.R. Novel scaffold hopping of potent benzothiazole and isatin analogues linked to 1, 2, 3-triazole fragment that mimic quinazoline epidermal growth factor receptor inhibitors: Synthesis, antitumor and mechanistic analyses. *Bioorganic Chem.* **2020**, *103*, 104133. [[CrossRef](#)] [[PubMed](#)]
47. Aouad, M.R.; Soliman, M.A.; Alharbi, M.O.; Bardaweel, S.K.; Sahu, P.K.; Ali, A.A.; Messali, M.; Rezki, N.; Al-Soud, Y.A. Design, synthesis and anticancer screening of novel benzothiazole-piperazine-1, 2, 3-triazole hybrids. *Molecules* **2018**, *23*, 2788. [[CrossRef](#)] [[PubMed](#)]
48. Aouad, M.R.; Almeahadi, M.A.; Rezki, N.; Al-blewi, F.F.; Messali, M.; Ali, I. Design, click synthesis, anticancer screening and docking studies of novel benzothiazole-1, 2, 3-triazoles appended with some bioactive benzofused heterocycles. *J. Mol. Struct.* **2019**, *1188*, 153–164. [[CrossRef](#)]
49. Sainsbury, J.R.; Farndon, J.R.; Needham, G.K.; Malcolm, A.J.; Harris, A.L. Epidermal-growth-factor receptor status as predictor of early recurrence of and death from breast cancer. *Lancet* **1987**, *1*, 1398–1402. [[PubMed](#)]
50. Salomon, D.S.; Brandt, R.; Ciardiello, F.; Normanno, N. Epidermal growth factor-related peptides and their receptors in human malignancies. *Crit. Rev. Oncol./Hematol.* **1995**, *19*, 183–232. [[CrossRef](#)]
51. Musa, A.; Ihmaid, S.K.; Hughes, D.L.; Said, M.A.; Abulkhair, H.S.; El-Ghorab, A.H.; Abdelgawad, M.A.; Shalaby, K.; Shaker, M.E.; Alharbi, K.S.; et al. The anticancer and EGFR-TK/CDK-9 dual inhibitory potentials of new synthetic pyranopyrazole and pyrazolone derivatives: X-ray crystallography, in vitro, and in silico mechanistic investigations. *J. Biomol. Struct. Dyn.* **2023**, 1–15. [[CrossRef](#)] [[PubMed](#)]
52. Ihmaid, S.K.; Alraqa, S.Y.; Aouad, M.R.; Aljuhani, A.; Elbadawy, H.M.; Salama, S.A.; Rezki, N.; Ahmed, H.E.A. Design of molecular hybrids of phthalimide-triazole agents with potent selective MCF-7/HepG2 cytotoxicity: Synthesis, EGFR inhibitory effect, and metabolic stability. *Bioorganic Chem.* **2021**, *111*, 104835. [[CrossRef](#)]
53. Othman, D.I.A.; Hamdi, A.; Tawfik, S.S.; Elgazar, A.A.; Mostafa, A.S. Identification of new benzimidazole-triazole hybrids as anticancer agents: Multi-target recognition, in vitro and in silico studies. *J. Enzym. Inhib. Med. Chem.* **2023**, *38*, 2166037. [[CrossRef](#)] [[PubMed](#)]
54. Elgaafary, M.; Fouda, A.M.; Mohamed, H.M.; Hamed, A.; El-Mawgoud, H.K.A.; Jin, L.; Ulrich, J.; Simmet, T.; Syrovets, T.; El-Agrody, A.M. Synthesis of β -Enaminonitrile-Linked 8-Methoxy-1H-Benzo[f]Chromene Moieties and Analysis of Their Antitumor Mechanisms. *Front. Chem.* **2021**, *9*, 759148. [[CrossRef](#)]
55. Ismail, N.S.M.; Ali, E.M.H.; Ibrahim, D.A.; Serya, R.A.T.; Abou El Ella, D.A. Pyrazolo[3,4-d]pyrimidine based scaffold derivatives targeting kinases as anticancer agents. *Future J. Pharm. Sci.* **2016**, *2*, 20–30. [[CrossRef](#)]
56. Kanopandian, N.; Li, D.; Kannan, S. Induction of intrinsic apoptotic signaling pathway in A549 lung cancer cells using silver nanoparticles from Gossypium hirsutum and evaluation of in vivo toxicity. *Biotechnol. Rep.* **2019**, *23*, e00339. [[CrossRef](#)]
57. Wilkins, R.C.; Kutzner, B.; Truong, M.; Sanchez-Dardon, J.; McLean, J. Analysis of radiation-induced apoptosis in human lymphocytes: Flow cytometry using Annexin V and propidium iodide versus the neutral comet assay. *Cytom. J. Int. Soc. Anal. Cytol.* **2002**, *48*, 14–19. [[CrossRef](#)]
58. Stamos, J.; Sliwkowski, M.X.; Eigenbrot, C. Structure of the epidermal growth factor receptor kinase domain alone and in complex with a 4-anilinoquinazoline inhibitor. *J. Biol. Chem.* **2002**, *277*, 46265–46272. [[CrossRef](#)]
59. Gaber, A.A.; Sobhy, M.; Turkey, A.; Abdulwahab, H.G.; Al-Karmalawy, A.A.; Elhendawy, M.A.; Radwan, M.M.; Elkaeed, E.B.; Ibrahim, I.M.; Elzahabi, H.S.A.; et al. Discovery of new 1H-pyrazolo[3,4-d]pyrimidine derivatives as anticancer agents targeting EGFR(WT) and EGFR(T790M). *J. Enzym. Inhib. Med. Chem.* **2022**, *37*, 2283–2303. [[CrossRef](#)]
60. Allouche, F.; Chabchoub, F.; Carta, F.; Supuran, C.T. Synthesis of aminocyanopyrazoles via a multi-component reaction and anti-carbonic anhydrase inhibitory activity of their sulfamide derivatives against cytosolic and transmembrane isoforms. *J. Enzym. Inhib. Med. Chem.* **2013**, *28*, 343–349. [[CrossRef](#)] [[PubMed](#)]
61. He, H.Y.; Zhao, J.N.; Jia, R.; Zhao, Y.L.; Yang, S.Y.; Yu, L.T.; Yang, L. Novel pyrazolo[3,4-d]pyrimidine derivatives as potential antitumor agents: Exploratory synthesis, preliminary structure-activity relationships, and in vitro biological evaluation. *Molecules* **2011**, *16*, 10685–10694. [[CrossRef](#)] [[PubMed](#)]
62. Mosmann, T. Rapid colorimetric assay for cellular growth and survival: Application to proliferation and cytotoxicity assays. *J. Immunol. Methods* **1983**, *65*, 55–63. [[CrossRef](#)] [[PubMed](#)]
63. Demirci, F.; Başer, K.H.C. Bioassay Techniques for Drug Development By Atta-ur-Rahman, M. Iqbal Choudhary (HEJRIC, University of Karachi, Pakistan), William J. Thomsen (Areana Pharmaceuticals, San Diego, CA). Harwood Academic Publishers, Amsterdam, The Netherlands. 2001. xii + 223 pp. 15.5 × 23.5 cm. \$79.00. ISBN 90-5823-051-1. *J. Nat. Prod.* **2002**, *65*, 1086–1087.

64. El-Mawgoud, H.K.A.; Fouda, A.M.; El-Nassag, M.A.A.; Elhenawy, A.A.; Alshahrani, M.Y.; El-Agrody, A.M. Discovery of novel rigid analogs of 2-naphthol with potent anticancer activity through multi-target topoisomerase I & II and tyrosine kinase receptor EGFR & VEGFR-2 inhibition mechanism. *Chem.-Biol. Interact.* **2022**, *355*, 109838.
65. Van Engeland, M.; Nieland, L.J.; Ramaekers, F.C.; Schutte, B.; Reutelingsperger, C.P. Annexin V-affinity assay: A review on an apoptosis detection system based on phosphatidylserine exposure. *Cytometry* **1998**, *31*, 1–9. [[CrossRef](#)]
66. Vermes, I.; Haanen, C.; Steffens-Nakken, H.; Reutelingsperger, C. A novel assay for apoptosis. Flow cytometric detection of phosphatidylserine expression on early apoptotic cells using fluorescein labelled Annexin V. *J. Immunol. Methods* **1995**, *184*, 39–51. [[CrossRef](#)] [[PubMed](#)]
67. Rosner, M.; Schipany, K.; Hengstschlager, M. Merging high-quality biochemical fractionation with a refined flow cytometry approach to monitor nucleocytoplasmic protein expression throughout the unperturbed mammalian cell cycle. *Nat. Protoc.* **2013**, *8*, 602–626. [[CrossRef](#)]
68. Morris, G.M.; Goodsell, D.S.; Halliday, R.S.; Huey, R.; Hart, W.E.; Belew, R.K.; Olson, A.J. Automated docking using a Lamarckian genetic algorithm and an empirical binding free energy function. *J. Comput. Chem.* **1998**, *19*, 1639–1662. [[CrossRef](#)]
69. Molecular Operating Environment (MOE) Chemical Computing Group, Quebec, Canada. 2012. Available online: <http://www.chemcomp.com> (accessed on 30 February 2013).

Disclaimer/Publisher’s Note: The statements, opinions and data contained in all publications are solely those of the individual author(s) and contributor(s) and not of MDPI and/or the editor(s). MDPI and/or the editor(s) disclaim responsibility for any injury to people or property resulting from any ideas, methods, instructions or products referred to in the content.